Emergent Materials (2020) 3:881–917
https://doi.org/10.1007/s42247-020-00116-y

REVIEW

A review of recent advances in water-gas shift catalysis for hydrogen production

Parisa Ebrahimi[1] · Anand Kumar[1] · Majeda Khraisheh[1]

Received: 16 May 2020 / Accepted: 15 July 2020 / Published online: 3 August 2020

Abstract

The water-gas shift reaction (WGSR) is an intermediate reaction in hydrocarbon reforming processes, considered one of the most important reactions for hydrogen production. Here, water and carbon monoxide molecules react to generate hydrogen and carbon dioxide. From the thermodynamics aspect, pressure does not have an impact, whereas low-temperature conditions are suitable for high hydrogen selectivity because of the exothermic nature of the WGSR reaction. The performance of this reaction can be greatly enhanced in the presence of suitable catalysts. The WGSR has been widely studied due do the industrial significance resulting in a good volume of open literature on reactor design and catalyst development. A number of review articles are also available on the fundamental aspects of the reaction, including thermodynamic analysis, reaction condition optimization, catalyst design, and deactivation studies. Over the past few decades, there has been an exceptional development of the catalyst characterization techniques such as near-ambient x-ray photoelectron spectroscopy (NA-XPS) and in situ transmission electron microscopy (in situ TEM), providing atomic level information in presence of gases at elevated temperatures. These tools have been crucial in providing nanoscale structural details and the dynamic changes during reaction conditions, which were not available before. The present review is an attempt to gather the recent progress, particularly in the past decade, on the catalysts for low-temperature WGSR and their structural properties, leading to new insights that can be used in the future for effective catalyst design. For the ease of reading, the article is divided into subsections based on metals (noble and transition metal), oxide supports, and carbon-based supports. It also aims at providing a brief overview of the reaction conditions by including a table of catalysts with synthesis methods, reaction conditions, and key observations for a quick reference. Based on our study of literature on noble metal catalysts, atomic Pt substituted Mn_3O_4 shows almost full CO conversion at 260 °C itself with zero methane formation. In the case of transition metals group, the inclusion of Cu in catalytic system seems to influence the CO conversion significantly, and in some cases, with CO conversion improvement by 65% at 280 °C. Moreover, mesoporous ceria as a catalyst support shows great potential with reports of full CO conversion at a low temperature of 175 °C.

Keywords Low-temperature water-gas shift · Catalyst nanostructure · Hydrogen production · CO conversion

1 Introduction

Fossil fuels have been continuously used as the primary source of energy for a long time. These resources are not renewable and pollute the atmosphere through greenhouse gases emission, which is linked to global warming. The depletion in fossil fuel reservoirs as well as the knowledge of their adverse environmental impacts has gained researchers attention to think about alternative and clean sources of energy [1]. Hydrogen is considered as a promising renewable alternative that minimizes CO_2 emissions and produces only water as a byproduct upon combustion [2]. Traditionally, among the non-fossil fuel-based methods, hydrogen has been produced by mixing iron (in the metal state) with strong acids, or using the well-established water electrolysis process. However, both techniques have some drawbacks, such as being costly to operate and not adequate to meet the growing market demands, which resulted in methane steam reforming being the most popular method for industrial-scale hydrogen production [3]. Recent research and development in the direction of alternative and sustainable energy production, such as wind energy,

✉ Anand Kumar
akumar@qu.edu.qa

[1] Department of Chemical Engineering, Qatar University, PO Box 2713, Doha, Qatar

solar energy, and geothermal energy, indicates that future energy demands will be met by a mixture of sources to decrease our dependence on fossil fuels. As the renewable energy becomes cheaper with time and starts to gradually dominate the energy market, diverse applications of existing hydrocarbons are being sought by converting them into more valuable chemicals and products rather than combusting them for energy production, which is not environmentally friendly and expected to be more expensive in the future.

The abundance of water and sunlight as affordable sources offers a good alternative for hydrogen generation. Hence, photocatalytic water splitting is considered to have a potential for sustainable production of hydrogen that can be employed in different scales of hydrogen generators [4]. For achieving high conversion efficiency in solar water splitting, photocatalysts should have some critical features such as high absorption of visible light, low charge recombination, and high surface reaction [5]. It is assumed that photocatalytic hydrogen is conceivable as a commercial fuel in the future, yet a considerable research is required in this area, addressing the aforementioned key points for manufacturing. The enhancement in photocatalytic performance is attributed to the presence of oxygen vacancies, which act as trapping sites via taking photogenerated holes or electrons that could be beneficial in the carrier's separation [6]. Furthermore, during the synthesis of photocatalysts, nanostructures and morphologies can be controlled to facilitate the generation of oxygen vacancies that efficiently raise the adsorption capacity and consequently make gas molecules (including O_2, N_2, H_2O, and CO_2) active [7]. Oxygen vacancies help promote hydrogen evolution reaction performance, due to their beneficial role in charge transfer and water molecule dissociation [8].

Hydrocarbons are converted to other chemicals, including hydrogen, by means of reforming processes in the presence of suitable catalysts. The WGSR, ubiquitous in reforming processes, is known to play a central role in adjusting hydrogen and carbon monoxide amount. In the WGSR, water reacts with CO to form hydrogen and carbon dioxide ($CO + H_2O \leftrightarrow CO_2 + H_2$), where the CO_2 can be separated from the stream to get pure hydrogen [9]. The WGSR is relevant to various industrial sectors, directly or indirectly, such as the fertilizer industry for the production of ammonia, petroleum refineries, and fuel cell for generating power as well as transportation applications [10]. This reaction is exothermic, which makes it thermodynamically suitable at lower temperatures [11]. Being exothermic in nature may lead the system to a thermally runaway condition at higher temperature if appropriate cooling arrangements are not made. The heat released will increase the temperature further accelerating the reaction and generating more heat. Hence, control and monitoring the temperature is mandatory in order to prevent such instability. Since the WGSR is an equilibrium-limited exothermic reaction, lower temperatures will favor more hydrogen production, however with slower kinetics [12]. Higher temperatures are more desirable for reforming reactions. Therefore, if a high ratio of H_2 to CO is needed and CO_2 in the reaction amount is larger than the stoichiometric value, higher temperatures are not favorable [13]. With the objective of enhancing the reaction performance, the WGS reaction has been studied by many groups using different catalysts, resulting in a substantial literature elucidating the catalysis and reactor design aspects. Some review articles are also available summarizing the effect of various parameters, such as reactants flow rate, temperature, and pressure on WGSR in the presence of catalysts [14–16]. Catalyst composition, metal-support interactions, porosity, and surface area effects have been widely reported; however, in our knowledge, a study relating the catalyst nanostructures with WGSR performance is still lacking. The microscopic imaging techniques have seen a remarkable improvement in the past few decades, enabling us to image and monitor the changes at nanoscale structures while performing catalytic reactions, with structural details leading to single-atom precision. This enhancement resulted in revealing valuable nanoscale insights that tend to affect the catalytic reactions significantly, leading to the emergence of novel research areas such as single-atom catalysts, tandem catalysts, and shape-size selective catalysts. We believe that a study is needed to collect and correlate the key developments relating the nanostructure information with catalytic performance, specifically for a ubiquitous reaction like WGSR with a high industrial significance. Herein, our aim is to provide a review of the recent progress in catalysts for low-temperature water-gas shift reaction over the last decade, with a primary focus on catalyst nanostructure analysis. In addition, we also aim to provide an overview of the recent development in catalyst preparation techniques, reaction conditions, supported catalysts design for WGSR.

2 Mechanism

Despite the simplicity of the reaction and extensive studies over the years, the WGS reaction mechanism is still controversial and complicated due to the sensitivity of the catalysts to minor changes in operational conditions. There are two prominent mechanisms for the WGS reaction: the regenerative (redox) mechanism and the associative (Langmuir-Hinshelwood) mechanism. Generally, at high temperatures, the WGS reaction is accepted to follow the redox mechanism, where CO molecule adorbs on the catalyst surface and abstracts one oxygen from the metal-oxide support to form carbon dioxide. Loss of oxygen from metal-oxide creates an oxygen vacancy that is fulfilled by dissociating a water molecule to generate hydrogen and oxygen atoms. Hydrogen atoms combine and desorb as hydrogen gas whereas oxygen atom is captured by the oxygen deficient metal-oxide [17]. The

associative mechanism, on the other hand, has been reported at low as well as high temperatures, usually proceeds by the adsorption of CO and H_2O on the catalysts surface leading to a reactive intermediate that subsequently decomposes to produce CO_2 and H_2 [18]. Nonetheless, the redox mechanism is still the most widely accepted mechanism for WGSR. Theoretically, Sun et al. combined DFT calculations with micro-kinetic analysis on Au/TiO_2 catalysts to conclude that the redox mechanism was the most plausible route for WGS [19]. Ammal and Heyden also reached the same outcome from their investigation on Pt/TiO_2 (110) catalysts, that both Pt clusters and single cationic Pt follow the redox mechanism [20]. This mechanism involves CO oxidation through obtaining atomic O from H_2O, via either two consecutive steps of H abstraction, or one H abstraction followed by two OH species disproportionation [21, 22]:

$$\begin{cases} H_2O + \text{Red} \rightarrow H_2 + \text{Ox} \\ CO + \text{Ox} \rightarrow CO_2 + \text{Red} \end{cases} \quad (1)$$

In this mechanism, the surface of the catalyst is successively oxidized by H_2O and then reduced by CO. Low temperatures are reported to be more favorable for hydrogen production, which is the primary objective and focus of this review article.

2.1 Catalysts in low-temperature water-gas shift catalysts

In order to facilitate the WGS reaction for a large scale of hydrogen production, choosing a suitable catalyst is important, which plays a central role in accelerating the reaction. A good catalyst would facilitate the adsorption of reactants on the surface of catalyst, their reaction, and desorption of the products to regenerate the active sites for the cyclic process of adsorption-reaction-desorption with new reactant molecules. An optimum interaction between gaseous molecules and catalyst surface is required as a weak interaction would result in low conversion due to quick desorption of the reactants, whereas a strong interaction could also result in low conversion and catalyst deactivation as the adsorbed molecules are too strongly bound to the surface leading to catalyst poisoning. These interactions are best understood in terms of volcano plots highlighting the optimum interactions leading to highest conversion of reactants. Figure 1 shows a 3D volcano plot for WGSR rate over the surfaces of transition metals as a function of the binding energies of atomic oxygen and carbon monoxide, formed on chemisorption-energy amounts on step sites. The presented model offers a good qualitative estimate of the relative order of activity of selected transition metal catalysts compared to the experiments. The figure reveals Cu to be the most active among the investigated catalysts, by being at the center with optimum adsorption energies for O and CO interactions [23].

Availability of oxygen vacancies, optimum strength for CO adsorption, and activity for water dissociation are some common characteristic roles of WGS catalysts [24]. In general, an ideal catalyst used for driving low-temperature WGS reactions should be cost-effective and CO-tolerant for large-scale uninterrupted operations as CO is known to have a poisoning effect on catalysts, even at an insignificantly low concentrations [25]. Besides, in terms of energy efficiency, the appropriate catalysts must be thermally stable and active at temperatures below 250 °C to provide reasonably high reaction rates. According to the literature, a wide variety of catalysts have been employed to reduce the overall cost of hydrogen production and enhance the low-temperature WGS reaction catalytic activity and stability. In the following sections, a comprehensive summary of the recent development on different types of catalysts used in low-temperature WGS reaction is presented. It includes the catalyst preparation method, the operation conditions, nature of catalyst support, along with the efficiency for hydrogen production. Our particular focus is on the nanostructure of the catalyst, which has not been extensively covered in previously reported reviews. The catalysts are classified based on the metals used as well as the type of support.

2.2 Type of active metal

2.2.1 Noble metal based

For commercial applications, any WGS catalysts should be free from some inherent disadvantages such as low stability and activity, along with the need for specific pretreatment and regeneration [26]. Chemically speaking, noble metals are well-known to be most resistant against corrosion and oxidation. Platinum (Pt), rhodium (Rh), gold (Au), palladium (Pd), and silver (Ag) are the commonly known noble metals, which have been extensively studied in recent years for WGS applications. The catalyst activity of the noble metals depend on many variables such as the method for catalyst preparation, noble metal amount, the support used, the amount, and characteristics of the prompter in case a promoter is used [27]. In multicomponent catalysts, the complex interactions between the metals and support also have a significant impact on the catalytic activity. Moreover, in the operation phase, the experimental variables like the space time, the reaction temperature, and the feed composition are influential [28]. The WGS catalysts activity of this group is known to depend on crystal size, dispersion, metal loading, metal oxide support, and the nature of the dopant used [27]; however, some contrary reports also exist indicating the activity of Pt/TiO_2 and Ru/TiO_2 not dependent on the metal loading or the crystallite size [29, 30].

Reducible oxides are reported to significantly improve the catalyst activity at low temperatures. Vecchietti et al.

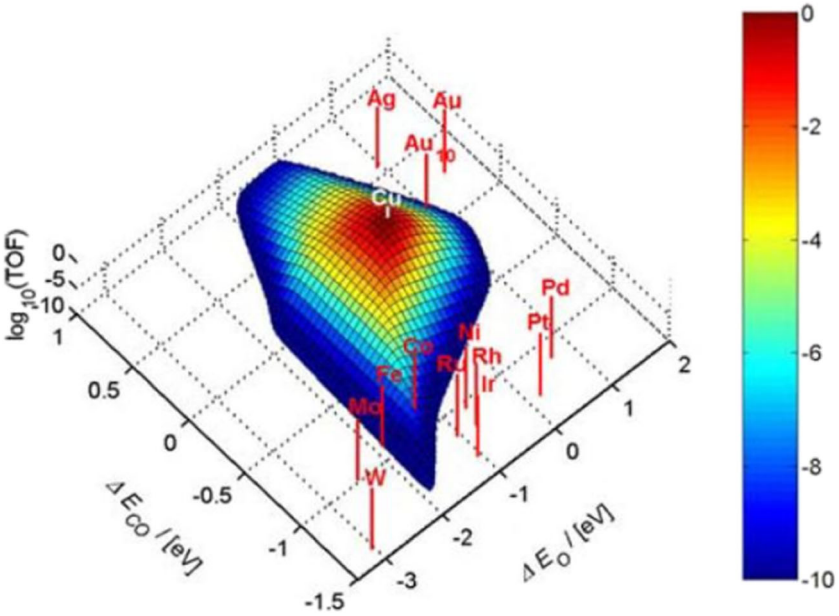

Fig. 1 3D volcano plot of the turnover frequency for the low-temperature WGSR vs O and CO adsorption energies [23]

discussed that water dissociation seems to be a critical step for reaction to move forward [31]. They studied the activation of water on oxygen vacancies on both pure as well as gallium-doped ceria supported platinum catalysts. The results showed a reverse correlation between the activity of the WGS catalyst and oxygen vacancies number [31]. In another study conducted by Tiwari et al., Pt nanoparticles with nanocrystalline CeO_2 support were investigated for low-temperature WGS reaction [32]. The 0.9Pt-CeO_2 (with 0.9 wt% Pt) catalyst showed the best activity (85.1%) with 1.66×10^{10} mol cm^{-1} s^{-1} CO_2 formation rate at 140 °C and 20,000 GHSV [32]. The nanostructure of the catalyst is shown in Fig. 2a–d, with HRTEM in Fig. 2c showing Pt crystallite size of 0.8 nm on spherical CeO_2 support of size between 40 and 50 nm [32]. Increasing the wt% of Pt resulted in an increase in Pt crystallite size as well as a lower surface dispersion of Pt of CeO_2, negatively affecting the overall catalytic performance, providing conclusive evidence of higher interaction between Pt and CeO_2 resulting in improved WGS activity [32].

Nguyen-Phan et al. investigated the performance of both Au- and Pt-based metal catalysts on hydrogen production through various conversion processes like WGS reaction [37]. The activity of Pt was concluded to be much higher compared to Au catalysts, where Pt was also susceptible to quick deactivation, possibly by CO poisoning or oxidation by water molecules [37]. Palma et al. presented a strategy to alleviate the challenges of Pt supported on Ce/Zr, suffering from deactivation caused by sintering and coking as well as high selectivity of methane [38]. They used wet impregnation method to synthesize supported bimetallic catalysts (Pt/M/$CeZrO_4$ (M = Na, Mo, Sn, Cu, Zn)) and compared their performance with monometallic ones. According to the result, in 473–675 K temperature range, 1Pt/1Sn/$CeZrO_4$ and 1Pt/1Na/$CeZrO_4$ showed similar CO conversion as Pt-based monometallic catalysts, however, with higher hydrogen production and reduced methane formation than the bimetallic systems. In general, the 1Pt/1Sn/$CeZrO_4$ catalyst had the best conversion and hydrogen selectivity at 480–673 K. At lower temperatures, however, the monometallic 1Pt/$CeZrO_4$ catalyst exhibited the best performance [38].

The use of supercritical fluid deposition (SCFD) is considered a promising catalyst preparation method, which has been recently highlighted in some studies. Deal et al. synthesized platinum catalysts on alumina support, both in the presence and absence of ceria by this method and tested them for WGS reaction [39]. The result of the analysis showed Pt to be in a highly dispersed form on the support. The CeO_x/Al_2O_3 pretreatment in H_2 before Pt deposition resulted in more Pt nucleation on Ce than in the non-pretreated support. However, the non-pretreated Ce-containing catalyst showed a more uniform particle size with the Pt nanoparticles enclosed in the crystallites of ceria. No methanation or deposition of carbon was witnessed in any of the experiments. Measuring the reaction rate confirmed that the catalyst was more active for WGS, with the rates per Pt mass exceeding the values reported in most literature for WGS reaction on the Pt-CeO_x catalysts. The high catalytic activity was attributed to the considerable amount of interfacial platinum/ceria contacts due to unique nanoscale interactions [39]. Kaftan et al. investigated KOH-coating Pt/alumina catalytic performance on WGS reaction [40]. They found that both activity and selectivity of the catalyst improved compared to the uncoated catalyst. Besides, the selectivity of CO_2 increased in the coated sample because of hydroxides and carbonates film formation on the catalyst surface [40]. González-Castaño et al. introduced a pre-catalytic buffer layer of CeO_2/Al_2O_3 oxides in Pt/CeO_2/

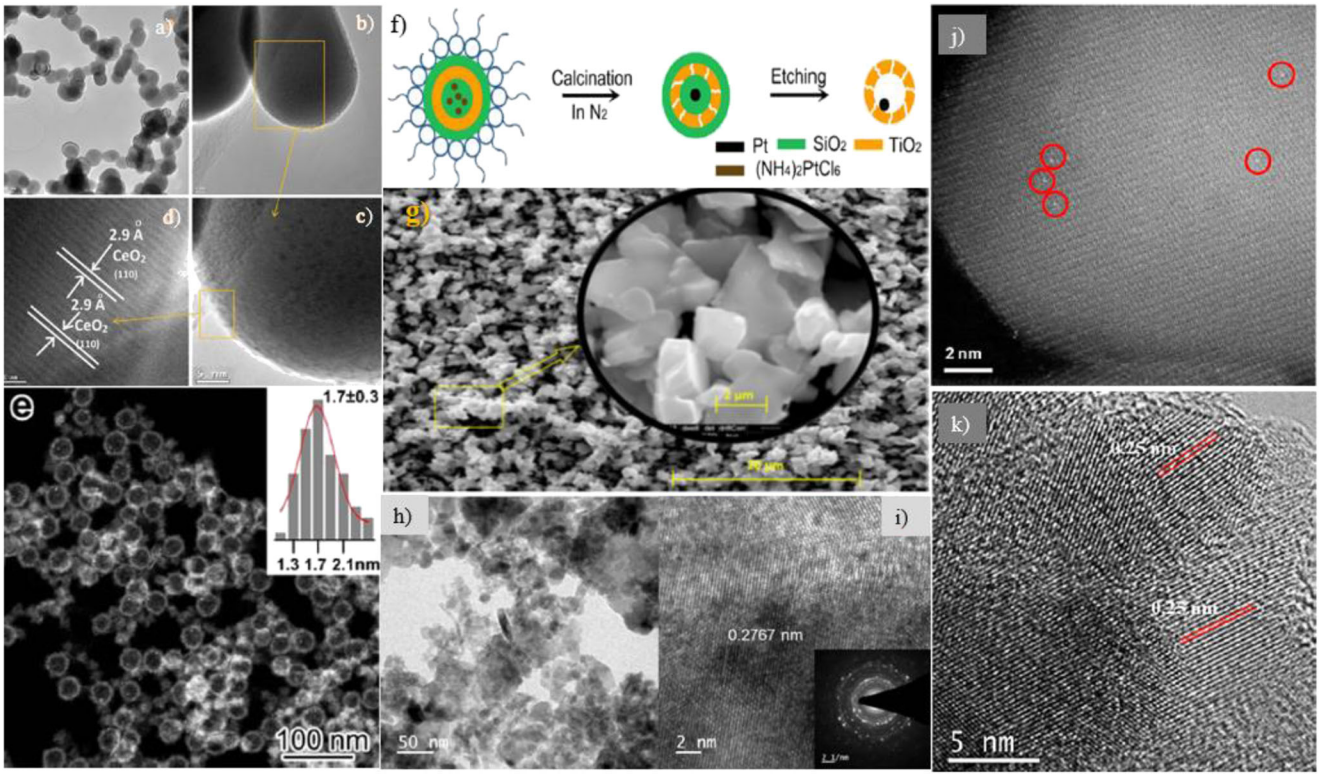

Fig. 2 **a**–**d** TEM images of the 0.9Pt-CeO_2 catalyst [32]. **e**, **f** HAADF-STEM images of the Pt@TiO_2 yolk/shell nanospheres and the Pt nanoparticles size distribution in the hollow TiO_2 nanospheres. Along with synthesis of the Pt@TiO_2 yolk/shell nanospheres [33]. **g** SEM image of the pure Mo_2C catalyst [34]. **h**, **i** Bright-field and HRTEM images of $Mn_{2.94}Pt_{0.06}O_{4-\delta}$ [35]. **j**, **k** AC-HAADF-STEM images of Pt/Fe-0.05 and HRTEM image of Pt/Fe-0.05 [36]

Al_2O_3 catalytic system for WGS reaction [41]. The inclusion of the buffer layer did not affect the CO oxidation; however, it increased the number of engaging sites during the reaction in the water dissociation phase leading to a catalytic activity enhancement in real conditions [41].

Recently, Pt-Re bimetallic clusters on TiO_2 support were reported to be a superior catalyst than Pt cluster alone for the low-temperature WGSR [42]. In order to understand the impact of both the Pt-Re clusters composition as well as Re oxidation, Duke et al. investigated a model system with bimetallic clusters grown on the surface of a rutile TiO_2 (110). The results showed that pre-oxidized clusters had lower activity in comparison to both unoxidized Pt-Re and pure Pt, which indicated that ReO_x sites are not active in the WGS reaction. Reduced CO poisoning in Pt-Re clusters demonstrated a higher WGS activity of the bimetallic clusters [42]. Synergistic effects at the interface of the metal-carbide are reported to cause a chemical activity enhancement for pure Pt, TiC, and MoC [43]. Rodriguez et al. found a correlation between Pt/MoC and Pt/TiC (001) water dissociation capability and their activity in the low-temperature WGS reaction. They found that both of these catalysts are highly active, stable, and selective with excellent catalytic performance. Moreover, small Pt coverage on the carbide substrates had the highest activity among the tested catalysts [43].

Pt nanoparticles with TiO_2 support have also been considered as an appropriate catalyst for the low-temperature WGS reaction, which exhibited the potential to be employed in a fuel cell system [33]. Zhao et al. published a synthesis strategy that affords uniform particles of Pt/TiO_2 with Pt nanostructures tunable size of around 1.0 to 2.6 nm incorporated in TiO_2 nanoshells of a thickness of ~ 3–5 nm and diameter of ~ 32 nm (Fig. 2e, f). These yolk/shell nanostructured catalysts were found to have remarkable stability, and their activity monotonically increased with the Pt nanoparticles size for the low-temperature WGS [33]. Rivero-Crespo et al. used water clusters to isolate and stabilize single atom Pt_1^{1+} that showed activity for WGSR at a low temperature of 50 °C [44]. They suggested that the water cluster could help in regulating the metal charge that facilitates the adsorption of reactants resulting in efficient low-temperature WGS catalysis, where a double water attack mechanism generates CO_2 with both oxygen coming from water [44].

The performance of Pt catalysts loaded on different supports, Mo_2C/η-Al_2O_3, Mo_2C/γ-Al_2O_3, or Mo_2C, were tested by Osman et al. for low-temperature WGS reaction [34], where Pt/Mo_2C/η-Al_2O_3 was found to be a promising catalyst with 44% CO conversion at 180 °C. However, 4 wt% Pt-Mo_2C (Fig. 2g) presented the highest catalytic activity and stable performance with 50% conversion at 180 °C and no

deactivation over 85 h of time on stream (TOS) at 250 °C temperature, maintaining over 70% CO conversion [34]. This improved performance was attributed to a uniform distribution of smaller Pt nanoparticles on Mo_2C structure compared to other supports. Recently, sonochemical synthesis has emerged as one of the useful methods for synthesizing metal oxides [45]. Anil et al. synthesized a series of noble metal substituted Mn_3O_4 catalysts via this method. All of the noble metal-supported Mn_3O_4 catalysts exhibited good activity for both low-temperature WGS and CO oxidation reactions. Atomic Pt substituted Mn_3O_4 ($Mn_{2.94}Pt_{0.06}O_{4-\delta}$), with the possibility of single-atom active sites (Fig. 2h, i), revealed excellent activity, with 99.9% conversion at 260 °C and no methane formation, owing to a strong interaction existing between Pt and Mn_3O_4 [35].

In order to design a metal-based catalyst with a high performance, identifying the effect of size at the atomic level is important. A comparative study on a series of Pt/FeO_x catalysts with two types of Pt, one as nanoparticles and the other as single atoms, was conducted by Chen et al. to evaluate the catalytic performance for low-temperature WGS reaction [36]. The results exhibited lower activation energy by Pt downsizing, and Pt single atom with 0.05 wt% loading (Fig. 2j, k) was found to be the most active catalyst with a CO conversion of ~ 65% at 300 °C [36]. In a theoretical study conducted by Fajín et al., the platinum nanotube performance was analyzed for the WGS reaction [46]. The authors suggested that Pt nanotube showed improved performance compared to the extended platinum surfaces or Pt nanoparticles deposited on metal oxides. Pt nanotubes were identified to be structurally more stable and avoided catalysts sintering in WGS reaction [46].

Pd is another well-known noble metal widely investigated for WGS reaction, as a single metal or in alloyed forms with other metals. Pd with different Co_3O_4 catalysts was investigated by Kono et al. for water-gas shift (WGS) reaction to produce hydrogen [48]. Palladium alone on cobalt oxide (Pd/Co_3O_4) exhibited low activity and higher methane selectivity; however, the Pd/K/Co_3O_4 as a catalyst with potassium loading > 0.78 wt% showed high activity for the WGS reaction. The potassium loading affected the CO species adsorption state, which caused Pd/K/Co_3O_4 catalyst to have high activity [48]. Sun et al. synthesized a series of Pd catalysts supported on FeO_x for WGS reaction and used Pd/Al_2O_3 as a reference for comparison [47]. They found that Pd/FeO_x showed a higher CO conversion compared to Pd/Al_2O_3 (Fig. 3a, b), and with high stability, even in the presence of CO_2 and H_2. Moreover, Pd single atoms can greatly enhance FeO_x reducibility and promote oxygen vacancies formation (Fig. 3c, d) [47].

Bulk gold is thought to be chemically inert; nonetheless, gold nanoparticles have revealed a high catalyst activity in the WGS reaction [49]. Bimetals of gold (Au-M, M = metals) on CeO_2 support were evaluated for WGS reaction where 3 wt% Au-Pt/CeO_2 showed high activity within a temperature range of 100–300 °C [50]. The WGS activity correlated well with the reducibility of ceria, that in turn was affected by the bimetallic cluster promoted local electronic band causing the stabilization of germinal OH groups, which were supposed to be responsible for enhanced WGS activity [50]. A comparative study was conducted by Castaño et al. on the performance of gold and platinum catalysts on ceria support [51]. Gold-based catalysts indeed showed a higher reaction rate at 180 °C; however, the activity of the catalysts was sensitive to temperature with Pt showing more activity at the higher temperatures. The gold catalysts had a high dispersion of 32% with an average crystallite size of 4 nm (Fig. 4a), that enabled Au to influence the electronic properties of the ceria support, which correlated with the activity for WGS reaction [51]. Later, the same group carried out a comparative study between Pt and structured gold catalysts, both supported on Fe doped ceria mixed oxide inserted onto metallic micro size monolithic structures (Fig. 4b, c) in order to find their performance in WGS reaction with O_2 assistance [52]. Pt was the most active metal in conventional conditions; nevertheless, in O_2 assisted WGS reaction, Au-based catalysts performed superior to Pt-based catalysts [52].

To understand the effect of the preparation method and the amount of Au on the catalyst activity in low-temperature WGS reaction, Soria et al. synthesized a series of nano-sized Au/Fe_2O_3 catalysts with several Au loadings and different synthesis methods [53]. The deposition-precipitation (DP) method with the Au content of 5 wt% (the highest tested loading) (Fig. 4d, e) was found to have the highest conversion of CO. Among the Au/Fe_2O_3 liquid phase reductive deposition (LPRD) samples, the most active catalyst was the one with the lowest quantity of Au (1.5 wt%) (Fig. 4f, g). Based on H_2-TPR analysis, the authors concluded that gold could promote Fe_2O_3 support reducibility, which seems to be a key factor in enhancing redox WGS reaction activity. In both, the DP and the LPRD methods, high dispersion of gold over the iron support with 2.2–3.1 nm crystallites was observed, and only an insignificant increase in the average particle size of used catalyst was witnessed after the reaction [53].

In another study, Reina et al. synthesized multicomponent catalysts including Au/$Ce_{1-x}Cu_xO_2$/Al_2O_3 and tested for WGS reaction to understand the role of each element; Au, Ce, and Cu; in the reaction [55]. The synergy between Cu-Ce and Au-support interactions greatly influenced the catalytic properties, and oxygen storage capacity. Though copper is an active catalyst for WGS reaction, gold was required to achieve a high conversion of CO. CeO_2 also played an important role, as both Cu and Au showed remarkable improvement in activity in the presence of CeO_2 with reasonable long-term stability [55]. Some studies have discussed that using bimetallic systems could improve both the activity and stability of the catalyst

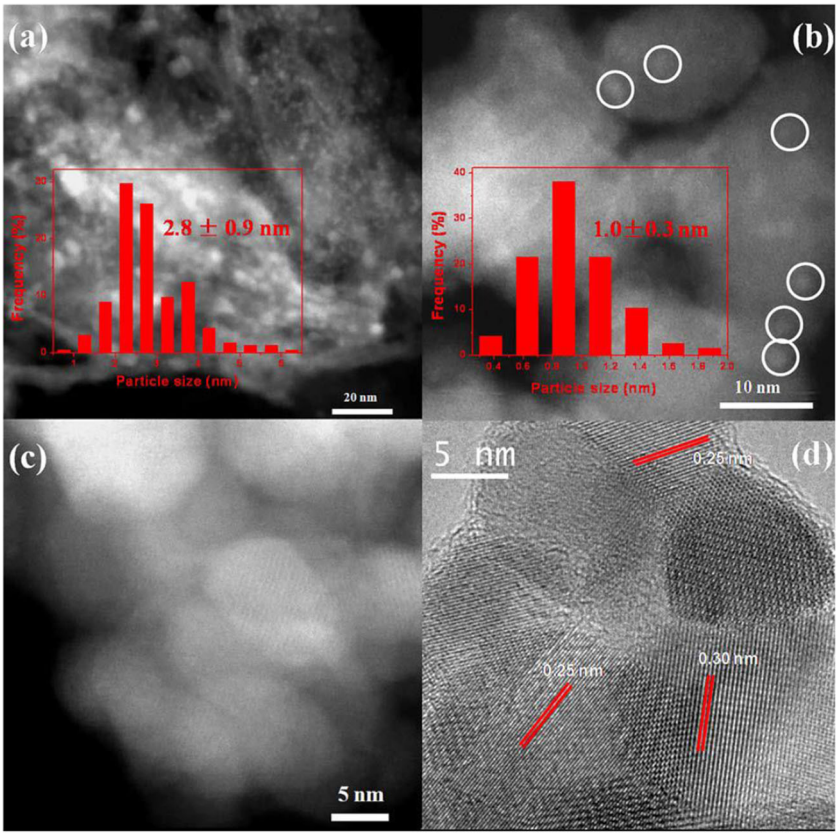

Fig. 3 **a**, **b** HAADF-STEM images of 1.3 wt% Pd/Al_2O_3 and 1.1 wt% Pd/FeO_x. **c**, **d** HAADF-STEM and HRTEM images 0.044 wt% Pd/FeO_x [47]

in the WGS reaction. For example, adding rhenium (Re) to Au catalysts with CeO_2 support significantly improved the catalytic activity [56]. Ozyonum et al. conducted an investigation on monolithic Au-Re/CeO_2 over microchannel cordierite [57]. They realized a relatively lower performance with Au/CeO_2 catalyst in comparison to the considerable improvement with Re addition as a promoter [57]. For achieving a high activity with Au-based catalysts for low-temperature WGS reaction, Yao et al. incorporated atomic layer deposition technique to grow clusters of layered gold on a molybdenum carbide (α-MoC) substrate to create an interfacial catalytic system for ultra-low-temperature WGS (Fig. 4h, i) [44]. This catalytic system was capable of dissociating water efficiently on the MoC surface as well as activating the CO on neighboring Ag clusters, resulting in high WGS activity at low temperature. Interestingly, even after the reaction, the sample still included both single-atom Au and layered Au clusters (Fig. 4j). The use of sodium cyanide (NaCN) solution has been effective in selectively leaching the layered Au clusters from in such systems (Fig. 4k) [54, 58].

Santos et al. examined the activity of gold nanoparticles catalyst combined with Cu/ZnO/Al_2O_3 for hydrogen production through WGS reaction [59]. This system could successfully achieve a full CO conversion at 180 °C due to the perfect synergy of gold and copper [59]. Fu et al. synthesized two different kinds of Au/Ce WGS reaction catalysts supported on the same nanorods of ceria, one with < 2 nm disordered clusters, and the other with 3–4-nm particles. The results exhibited that the disordered gold clusters had superior activity than the nanoparticles of gold [60]. Stere et al. utilized non-thermal (cold) plasma activation to facilitate low-temperature WGS reaction over an Au-based/$CeZrO_4$ catalyst, where they concluded that the catalyst activity was comparable to that achieved through heating the catalyst up to 180 °C [61]. Santos et al. performed an investigation to optimize the performance of the Au/Cu-ZnOAl_2O_3 catalytic system by applying various ratios of active components as well as the Au preparation methods [62]. This system not only had a high carbon monoxide conversion but also showed stability during the start/stop operations as well as for long-term TOS, which is a prerequisite in real applications. It was concluded that combining Au with commercial-like Cu-Zn-Al compounds by hydrotalcite process can generate a new series of catalysts for WGS reaction with the capability to develop large scale hydrogen production technologies [62]. Au-based catalyst supported on Ce-Zr has been considered as one of the most active low-temperature WGS catalysts recorded to date; however, in the reaction conditions, a rapid deactivation occurs [63, 64]. Carter et al. evaluated a series of Ce-Ti support that were synthesized by the sol-gel method. They supported Au on these mixed metal oxides via a deposition-precipitation method, intending to resolve the deactivation issue. The

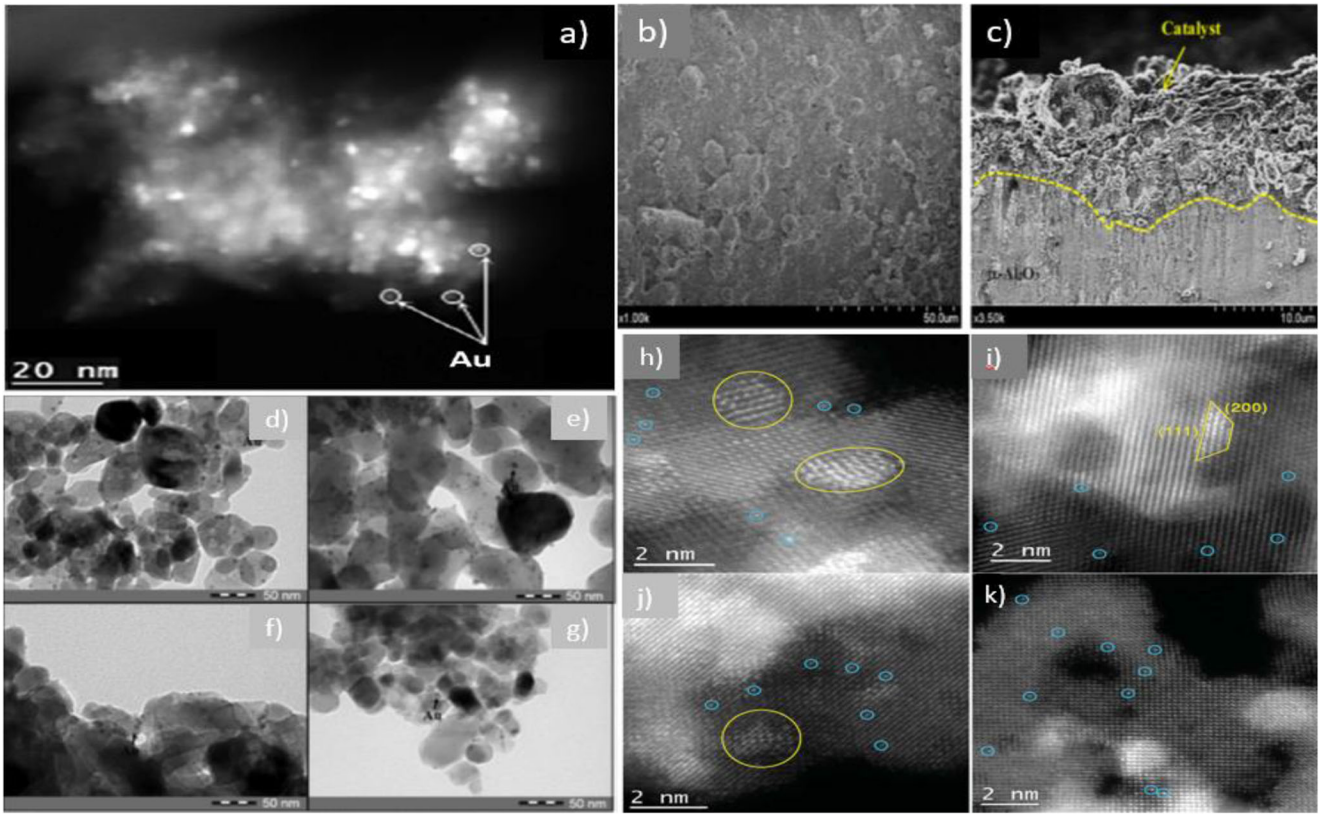

Fig. 4 **a** HAADF-STEM images of Au/CeFeAl [51]. **b**, **c** SEM micrographs of the micro monoliths Au/CeFe catalyst: **b** front; **c** cross-section view [52]. HRTEM images of **d**, **e** the $5Au/Fe_2O_3$ DP fresh and used (**f**, **g**) $1.5Au/Fe_2O_3$ LPRD fresh and used catalysts, respectively [39]. HAADF-STEM images of **h**, **i** fresh (2%) Au/α-MoC, **j** used (2%) Au/α-MoC, and **k** the (2%) Au/α-MoC catalyst after NaCN leaching, representing predominantly Au single atoms in which most of them overlapped with Mo sites in the support lattice (very bright features were created by overlapping MoC particles. (Blue circles: Au single atoms, yellow highlights: layered Au structures) [54]

results of low-temperature WGS reaction showed high activity and stability for $Au/Ce_{0.2}Ti_{0.8}O_2$ compared to ceria-zirconia due to the highest specific surface area represented by amorphous $Ce_{0.2}Ti_{0.8}O_2$ and well-dispersed of Au species [65].

The use of a suitable Rh single-atom catalyst (SAC) could make the WGS performance very active and selective in terms of adsorption and reaction. SAC is now considered a new dimension in heterogeneous catalysis that presents a very high dispersion of metal species, in atomic form, and reported to display optimum catalytic properties in many cases [67]. Guan et al. reported a Rh_1/TiO_2 SAC with a loading amount of 0.37 wt%, resulting in an overall 95% CO conversion with no methanation at 300 °C, which is viable even in a WGS stream rich with CO_2 and H_2 [66]. The result suggested that Rh single atoms enhanced the oxygen vacancies formation on TiO_2 support in order to generate more H_2 than Rh clusters. Besides, the SAC activity was about four times higher than the cluster catalyst with no formation of methane. The single atoms of Rh and nanoclusters were verified by HRTEM, as shown in Fig. 5 [66]. Mandapaka et al. synthesized Rh and aluminum co-doped ceria catalysts by a single-step solution combustion synthesis technique and tested its reactivity for WGS reaction and CO oxidation. The results showed that the bimetallic Rh and Al doped catalyst yielded a higher activity and surface area than the single metal doping of Rh/Ce and Al/Ce synthesized by the same method [68].

The catalytic performance in heterogeneous catalysts is affected by the dispersion of the active precious metal, and frequently, the active sites coalesce and grow during the reaction that result in lower activity over a longer time of analysis. Homogeneous catalysts, on the other hand, are known for high turnover frequency due to availability of atomic level sites. Ruthenium-based homogeneous catalysts have been particularly investigated for WGS reaction. Metal carbonyls, e.g., ruthenium-carbonyl, catalysts are low-cost homogeneous catalysts, which have been reported to operate at a lower temperature than the heterogeneous catalyst systems resulting in higher equilibrium conversion [70]. However, these systems require a high CO pressure, above 10 bar, and in this regard, volatile solvents and ionic liquid (IL) have been considered. Huang et al. reported that Ru-iongel catalysts show better activity and stability for low-temperature WGS reaction in comparison to the catalysts with supported ionic liquid (IL) phase, possibly because of a strong interaction between silica support and IL. The iongel catalyst activity increased with

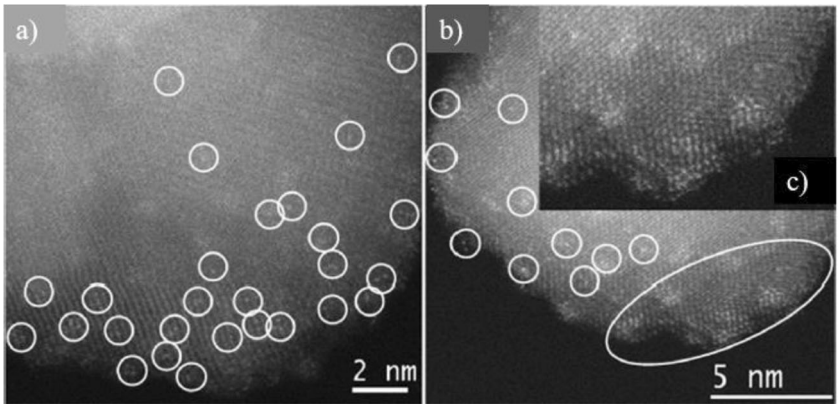

Fig. 5 **a** HAADF/STEM images of 0.37Rh/TiO_2-AL. **c** Enlarged district in **b**, showing the loosely Rh species single-atom dispersion. (White circles: Rh single atoms, red circles: Rh clusters) [66]

increasing the IL loading, and the larger anions iongel catalysts showed higher activity in the WGS reaction [71]. The effect of adding K_2CO_3 on the Ru/C catalysts performance (Fig. 6a) was investigated by Liu et al. through the positive reduction method by three different agents, $NaBH_4$, ethylene glycol (EG), and H_2, in which the Ru/C catalyst reduced by H_2 exhibited the highest catalytic activity for WGS reaction (Fig. 6b). The alkali additives showed a strong adsorbed gas bonding that improved the catalytic activity of the Ru/C. It also resulted in a concentration balance of water and CO on the active sites [69]. Queiroz et al. likewise studied the performance of 2% Ru/C for the low-temperature WGS reaction in a fixed bed reactor that resulted in 80% CO conversion under the steady-state condition at 553 K [72]. Later, they examined the catalytic performance of Ru during the low-temperature WGS reaction with two different supports, TiO_2 and Al_2O_3. The result showed that at 573 K, CO conversion on both Ru/Al_2O_3 and Ru/TiO_2 catalysts stayed 85% in a steady-state condition [73]. Queiroz et al. developed a WGS process with a membrane reactor using 2 wt% Ru on TiO_2 catalyst at 453–573 K and atmospheric pressure [74]. The result of the experiments at 573 K, both with and without permeation, showed 90 and 75% CO conversion, respectively. Besides, the results showed a 75–96% hydrogen recovery in the permeation operation, which was ~ 5 times higher than the operation without hydrogen permeation [74]. Supported ionic liquid phase (SILP) materials have been used to perform reactions at a low-temperature range [75, 76]. Stepic et al. successfully used this approach to enable a highly effective, homogeneously dispersed Ru-based catalyst to perform WGS reaction in the temperature range of 100 °C and 150 °C [77].

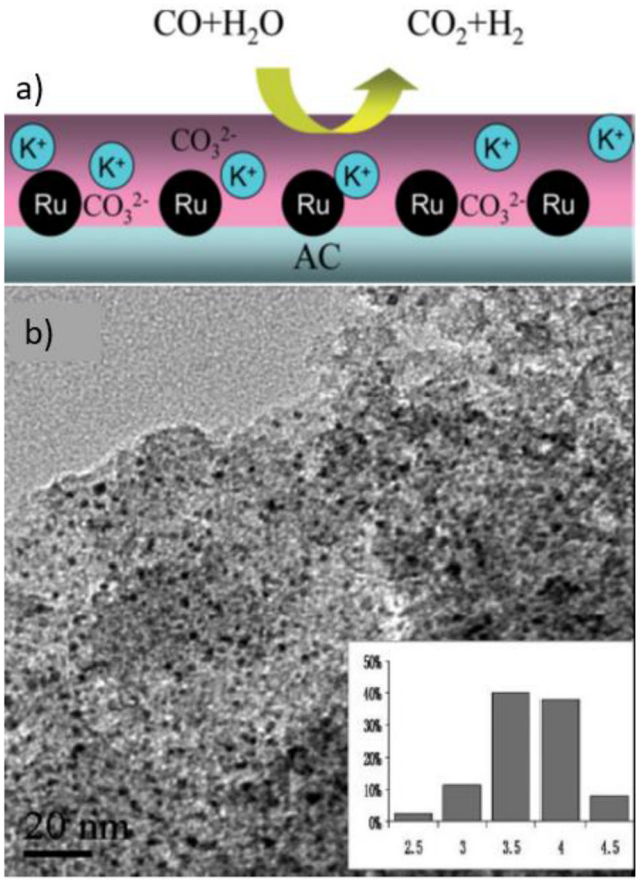

Fig. 6 **a** The WGS mechanism of the K_2CO_3 additive Ru/C catalyst, **b** TEM images of Ru/C catalysts reduced H_2 and an estimation of size distributions [69]

From this section, it is clear that noble metals have been extensively studied for WGSR. The dispersion of the active metal and the reducibility of the metal oxide support seem to be the key parameters affecting a catalyst's performance. The use of the SCFD method, as well as sonochemical preparation techniques, seems to offer a good control over nanoscale dispersion of the noble metals on the support leading high turnover numbers. In the case of Pt-containing supported catalyst, washing with a base, like KOH, helps in improving the catalyst performance for WGSR. The presence of gold, alone or with other noble metals, is shown to affect the reducibility of CeO_2 as well as FeO_x, which in turn positively affects their performance. Single-atom catalysts of Pt and Au supported on CeO_2 perform exceptionally well, which can further be improved by promoting the catalyst with single-atom sites of Re.

Next, we review the progress in transition metal catalysts, which offer economic alternatives to the noble metals.

Supported catalysts composed of Cu, Zn, Ni, and Co, alone or alloyed, have been investigated broadly for WGSR and offer to have good activity and selectivity for the low-temperature reaction.

2.2.2 Transition metal catalysts

Transition metals are elements from groups 3 to 12 in the periodic table, and they are known for their catalytic properties for many reforming reactions. Inclusion of transition metals such as Fe, Cu, and Zn as dopants in CeO_2 for gold supported ceria catalysts ($Au/CeO_2/Al_2O_3$) is reported to improve the performance for WGSR [78]. Transition metals tend to increase the redox properties and promote structural stability. Herein, we present some of the transition metal-based catalysts for WGSR.

Previous sections indicate that Au nanoparticles act as suitable catalysts for the oxidation of CO; however, some authors argue that water dissociation and adequate WGS reaction rate on pure Au are challenging to achieve. Copper, on the other hand, is reported to be more active for WGS reaction, although a significant barrier in Cu activation is required to be overcome for water dissociation [79]. Saqlain et al. studied the behavior of two different catalysts, Cu (100), and bimetallic Cu-Au (100) [80]. Results indicated that the dissociation of water for the Cu (100) and bimetallic surfaces were spontaneous up to 229 K and 520 K, respectively. In terms of reactivity, the study suggested that the bimetallic surface was far more reactive compared to the Cu (100) surface [80]. In another study, Wijayapala et al. used catalyst systems Mo/Co/K/ZSM-5 and Mo/Ni/K/ZSM-5 (ZSM-5 = zeolite), alone and with a copper-based WGS catalyst, for CO/H_2 ratios conversion in a batch reactor into aromatic hydrocarbons. The presence of Cu in the WGS catalyst system significantly improved CO conversion from 25 to 90% at 280 °C [81]. Jeong et al. reported a strong effect of support on catalytic activity in copper-based WGS catalyst [82]. In this regard, they tested Cu/CeO_2 catalysts prepared by incipient wetness and co-precipitation methods and optimized the copper loading in order to get a highly active Cu/CeO_2 catalyst. Results indicate that the catalysts prepared by co-precipitation (Fig. 7a) had superior performance with highest CO conversion and 100% CO_2 selectivity in addition to easier reducibility [82]. Camara et al. investigated the low-temperature WGSR mechanism on CeO_2/Cu catalysts using *operando* SSITKA-DRIFTS-mass spectrometry, where they identified a specific type of carbonate intermediate (bi or tridentate), which was believed to be the rate-limiting intermediate controlling the formation of CO_2 [83]. Moreira et al. studied the sorption enhanced WGS reaction at low-temperature (125–295 °C) over Cu-CeO_2/HTlc catalysts, where they reported a 70% volume enrichment in hydrogen and improved CO conversion upon efficient removal of CO_2 from the effluent stream [84]. Cu supported on nanoparticles size polyhedral ceria, with 87.6% CO conversion, was found to have the highest activity in comparison to other catalysts reported in this work [84].

Jeong et al. prepared Cu-CeO_2, Cu-ZrO_2, and Cu-CeO_2-ZrO_2 to obtain feasible catalysts for low-temperature (200 to 400 °C) WGS reaction. The cubic Cu-$Ce_{0.8}Zr_{0.2}O_2$ catalyst showed the highest CO conversion maintaining a stable TOS performance for 100 h with no significant loss in the activity [85]. Price et al. proposed a design strategy to overcome the limitations of large residence time requirement for Cu-based catalysts in WGS reaction [86]. They synthesized a series of Cu-ZnO catalysts with different supports and evaluated their performance. The results indicate that CeO_2-Al_2O_3 support can work under medium to high space velocities while maintaining a high activity and long-term stability [86]. Lang et al. introduced copper/ceria/foam catalysts to perform WGS reaction at a temperature range of 150 to 300 °C and GHSV between 3600 and 9500 h^{-1} at the outlet of a biomass gasifier with a limited pressure drop. The optimum amount of Cu and Ce resulting in the highest catalytic activity were 5.5 and 9.0 wt% respectively on a 30 ppi porosity foam [87]. Dalin Li et al. developed $Cu/ZnO/Al_2O_3$ catalysts with various compositions of Cu-Zn-Al layered double hydroxides (LDHs) for WGS reaction [88]. The formation of 2–6 nm size Cu with a dispersion percentage of 18–48% was observed after the reduction. The results showed that the 30%Cu/Zn_1Al catalyst had the highest activity, thermal stability, and long-time catalytic stability compared to the commercial catalyst of $Cu/ZnO/Al_2O_3$ [88]. Zhang et al. used uniform nanocrystals of Cu to investigate the Cu actives site for low-temperature WGSR [89]. The results indicated that Cu cubes with (100) exposed facets, in contrast to Cu octahedral enclosed with (111) facets, are active up to 548 K. Therefore, it was concluded from this study that Cu cubes-supported on ZnO had an extremely high activity for low-temperature WGSR [89]. Yan et al. reported a bulk promoted Cu-Fe_3O_4 catalysts for low-temperature WGS reaction, where the interaction between Cu and Fe helped in stabilizing and significantly improving the Cu^0 dispersion that resulted in an increased activity for WGS CO conversion. The Fe addition promoted both CO and H_2O adsorption. Different compositions of Cu and Fe were investigated and the $Cu_{0.3}Fe_{0.7}O_x$ catalyst showed a high initial activity that deactivated after 26 h; thereafter, $Cu_{0.7}Fe_{0.3}O_x$ surpassed the $Cu_{0.3}Fe_{0.7}O_x$ activity. Moreover, the inclusion of alumina in the multicomponent Cu-Fe_3O_4-Al_2O_3 catalyst resulted in superior performance, improved activity, and long-term stability compared to the catalysts without alumina in the structure (Fig. 7b) [90].

Coal gasification, which inherently involves WGS, is considered a clean hydrogen production method to convert coal resources into chemical energy; however, the process is still costly. In this regard, Zhao et al. adopted a solar-driven WGS method to significantly decrease the consumption of energy

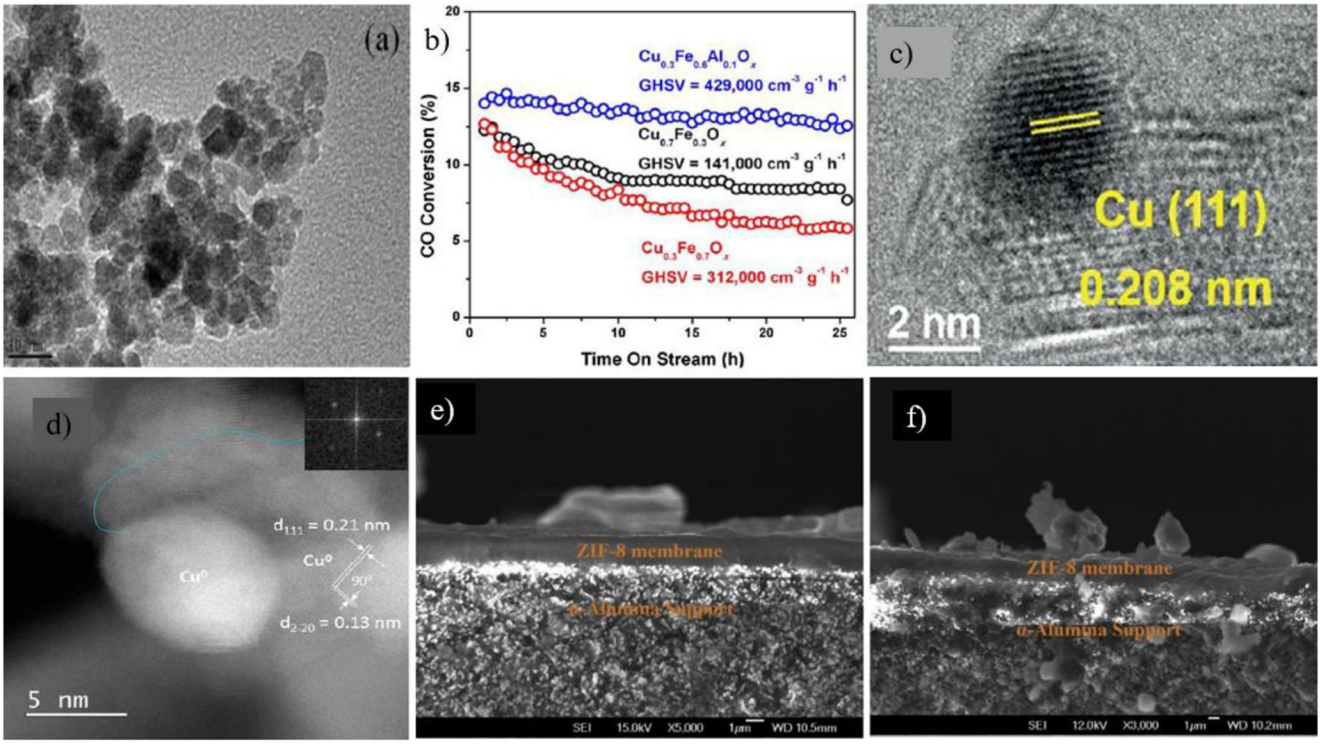

Fig. 7 **a** TEM image of fresh co-precipitated $CueCeO_2$ [82]. **b** Time on stream-dependent CO conversion of $Cu_{0.3}Fe_{0.7}O_x$, $Cu_{0.7}Fe_{0.3}O_x$, and Cu-Fe_3O_4-Al_2O_3 [90]. **c** HRTEM of CuO_x/Al_2O_3 catalyst [91]. **d** High-resolution STEM image with inset of EDX of the Cu/Fe_3O_4 rods [92]. **e**, **f** The cross-sectional SEM images of the ZIF-8 membrane **e** before and **f** after use [94]

[91]. They found that the CuO_x/Al_2O_3 (Fig. 7c) delivered 122 $\mu molg_{cat}^{-1}$ s^{-1} H_2 evolution and more than 95% CO conversion under light irradiation, that was more efficient than Au/Al_2O_3 and Pt/Al_2O_3. Apart from no cost for electric/thermal power, this solar-driven WGS process was capable of converting 1.1% light-to-energy [91]. Ma et al. synthesized Cu/Fe_3O_4 catalysts with nanorod structure using aqueous precipitation method (Fig. 7d), which showed good activity for high-temperature WGS reaction but did not show much activity at low temperatures [92]. The authors conducted ambient pressure XPS (AP-XPS) analysis and identified Cu^+ as the dominant, and possibly active phase, for WGSR.

To investigate the role of preparation method on the structure and catalytic activity in WGSR, Farzanfar et al. synthesized $Cu\text{-}Mn/SiO_2$ catalysts with three different methods [93]. The results determined that thermal decomposition of the inorganic complex was more suitable compared to impregnation and co-precipitation methods for developing active and stable $Cu\text{-}Mn/SiO_2$ WGS catalysts for 180–320 °C temperature range [93].

Kowalik et al. studied the impact of the hydroxycarbonate-assisted precipitation media on the physicochemical properties and activity of $Cu/ZnO/Al_2O_3$ system in low-temperature WGS reaction [95]. They employed water, glycol, and aqueous ethanol solution as the reactive medium. The results revealed that the alcohol assisted method could lead to a $Cu/ZnO/Al_2O_3$ catalysts with higher catalytic activity and stability than the other conventional techniques [95]. A comprehensive investigation was performed by Yin et al. to illustrate the beneficial characteristics of a zeolitic imidazolate framework-8 (ZIF-8) reactor (Fig. 7e, f) and $Cu/Zn/Al_2O_3$ catalysts for a low-temperature WGS reaction [94]. The membrane reactor exhibited 9.2×10^{-7} mol/m^2 s·Pa hydrogen permeance, which was much higher than the conventional metal and zeolite membranes, making it more attractive for practical hydrogen production. In addition, at a low temperature of 120–220 °C, the CO conversion using the ZIF-8-based membrane reactor was 13.5% higher than the conventional packed reactor [94]. Despite the high gas permeance of ZIF-8 membrane with considerable H_2 perm-selectivity, due to the low hydrothermal stability of materials used in this membrane, the system needs further improvements to make it more suitable for WGS reaction conditions [96, 97].

To evaluate the Fe-doping effects on the catalyst performance, Chen et al. synthesized $Fe\text{-}Ce\text{-}O_x$ composite oxides, consisting of CeO_2 nanorods and Fe_2O_3 nanoparticles, and applied them in the WGS reaction [98]. The results of the analysis revealed that introducing Fe^{3+} into CeO_2 crystal lattice structure increased the catalytic activity for the WGS reaction. It was also concluded that the reducing gas atmosphere synthesis method was more favorable for enhancing the doping effect. However, the catalyst was more active at high temperature and the CO conversion increased when the temperature was increased from 300 to 500 °C [98]. The effect of Fe-

Ce-O_x composite oxides had also been studied by other groups showing high catalytic activity towards WGS reaction [99].

With the objective of studying the impact of alkali-I metals promotion, such as Li, Na, K, Rb, and Cs, on both activity and stability of Co_2C for the low-temperature WGS reaction, Gnanamani et al. performed a study at 453 to 573 K and atmospheric pressure and compared the results with the unpromoted Co_2C reference catalyst [99]. The WGS reaction results indicated the unpromoted cobalt carbide to be active, although the catalyst deactivated over longer TOS due to the chemical transition of carbides to metallic form during the WGS reaction. However, the potassium promoted catalyst presented higher activity and better stability compared to the rest of the alkali supported Co_2C catalysts [100].

Chen et al. studied the intrinsic activities of Co-promoted MoS_2 and unpromoted-MoS_2 on Co-MoS_2/Al_2O_3 for WGSR, and reported a lower activation energy for Co-promoted sites [101]. The Co-promoted MoS_2/Al_2O_3 is widely used in hydrogen production industries as a catalyst for WGS reaction in the presence of sulfur [101].

Recently, Alamolhoda et al. worked on understanding the synergetic effect between nickel and cerium as catalysts in WGS reaction, and reported the use of low percentage loading (0–3 wt%) of cerium and nickel as dispersed phases on MFI framework [102]. According to the results, the cerium only catalysts had shown no sign of reaction, whereas the single metal Ni-MFI series catalysts successfully activated the CO. The prepared Ni-Ce-MFI succession had together speeded up the WGSR even at a low temperature of 503 K, and in some cases, the equilibrium conversion was achieved at temperatures less than 548 K. The presence of ceria is believed to provide the oxygen required for promoting nickel activity, which was clear from the TPR profile requiring lower temperature for nickel reduction in Ni-Ce-MFI catalysts. The lowest reduction temperature was observed when Ni and Ce were present in equal weight percentages [102]. Iriarte-Velasco et al. used calcined pork bone, composed mainly of hydroxyapatite (HAp), as support for transition metals for WGSR [103]. Both activity and selectivity were studied and correlated with the catalytic properties. The catalytic activity was observed to follow a trend: Ni > Co > Cu > Fe. Moreover, compared to the synthetic hydroxyapatite, the natural support showed a lower Ni methanation activity and increased long-term stability [103].

From this section, it is clear that transition metals can be a good choice for low-temperature WGS reaction. Bimetals and alloys, particularly of Cu and Zn, in some cases are reported to offer better performance than single metal catalysts. Transition metals normally enhance the redox properties of the catalyst that helps in improving the activity and long-term stability. Addition of alkali metals is also reported to enhance the activity by facilitating the adsorption and dissociation of the water molecule, which tend to be an energy-consuming step for most of the transition metals. Transition metal carbides (e.g., Co_2C), sulfides (MoS_2) are also reported to perform well for low-temperature WGS reaction. Throughout the previous section related to catalysts, the function of support is found to be quite instrumental in defining the performance of the catalyst. The next section presents a review on the role and recent development in catalyst supports for WGSR. This part is divided into two categories, metal oxide supports and carbon-based supports, for the ease of reading.

2.3 Type of metal oxide support

Ceria has been broadly investigated as a support to disperse the noble metals active sites in WGS reaction. CeO_2 supported catalysts have shown effective performance with effluent gas streams resulting in low CO concentrations. Cerium is known to have dynamic oxidation states which can change easily during reaction conditions. Besides, it also has a high oxygen movement and vacancy [104]. Jain et al. investigated the potential of three distinct Pt/Ceria catalysts at 150–450 °C with a GHSV of 13,360 h^{-1} to determine the impact of processing techniques and surface area, as well as porosity and crystallite size of ceria on the rate of WGS reaction [105]. In this work, the mesoporous ceria with a crystallite size of 5.8 nm and synthesized via sol-gel method was found to be the best catalyst with a complete conversion of CO at 175 °C (Fig. 8a–c) [105]. Byun et al. prepared a series of Cu-ZnO-CeO_2 catalysts to investigate the influence of CeO_2 addition on low-temperature WGS reaction performance [106]. These catalysts included a fixed amount of Cu (50 wt%) and different ceria content (from 0 to 40%), which affects the Cu dispersion and binding energy. The result showed that a 10 wt% cerium could promote catalyst reduction and CO conversion at low temperatures of 200–400 °C [106]. Petallidou et al. also investigated the effect of three synthesis methods (sol-gel, pechini, and urea co-precipitation) on 0.5 wt% Pt/$Ce_{0.5}La_{0.5}O_{2-\delta}$ (Ce: La = 1:1) catalyst and used different characterization techniques, such as in situ Raman, temperature-programmed techniques (TPD-H_2, TPD-NH_3, TPD-CO_2), powder XRD, and oxygen storage capacity (OSC), to thoroughly analyze the properties of the synthesized catalysts. The results revealed that Pt/$Ce_{0.5}La_{0.5}O_{2-\delta}$ synthesized by urea co-precipitation had the highest CO conversion activity compared to the other two methods [107].

Schilling and Hess investigated CeO_2 support for Au catalyst using *operando* Raman spectroscopy to understand the role of bulk and surface oxygen in the WGS reaction [111]. They concluded that the presence of 0.5 wt% Au/CeO_2 catalyst could successfully reduce the Ce support under WGS conditions. Results also revealed the dominant mechanism of the reaction to be the redox-type [111]. The use of

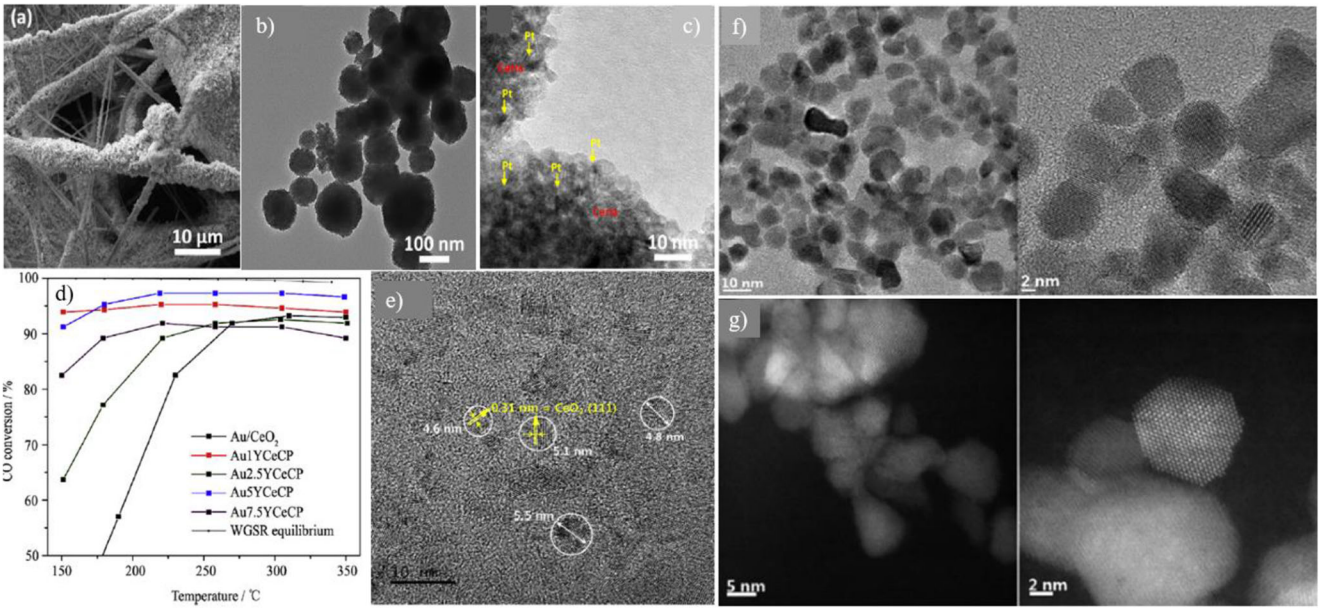

Fig. 8 **a**–**c** Electron microscopy analysis of Pt/ceria catalysts prepared by sol-gel after WGS testing [104]. **d** Temperature dependence of the CO conversion over Au catalysts on Y-doped Ce synthesized by CP [107]. **e** TEM images of the Cu/CeO_2 catalysts prepared by reverse precipitation method [108]. **f** TEM and HRTEM images of CuO/CeO_2 (ns), **g** STEM and HRSTEM images of CuO/CeO_2 (ns) [109]

mesoporous ceria, both as a catalyst and as a support, is widely seen for different reactions due to a large amount of specific surface area, well-developed nanocrystalline framework, and excellent surface oxygen vacancy compared to the bulk form of ceria [112]. In a study conducted by Li et al., an ordered mesoporous series of ternary metal oxide Cu-Mn-Ce were synthesized using a nano-casting method [113]. It was found that among the tested catalysts, the $Cu_{0.18}Mn_{0.02}Ce_{0.8}O_2$ mesoporous catalyst had the highest activity with almost 100% CO conversion for low-temperature WGS reaction without any methane production. Moreover, the catalyst was tested for 16 h TOS with no significant activity loss [113]. In order to understand the effect of modifying ceria by Y_2O_3 rare earth on the WGS reaction activity of Au/ceria, a study was conducted by Tabakova et al., in which all the designed catalysts, except for $Au_{2.5}YCe$ synthesized by co-precipitation method, showed > 90% CO conversion at 180–220 °C (Fig. 8d) [108].

Ceria with less than 10 nm particle size with exposure to WGS environment containing H_2O show high densities of adsorbed -OH group resulting in hydroxylated ceria nanoparticles [114]. Huang et al. showed that hydroxylated ceria nanoparticles are active for WGS reaction without requiring any metal cocatalyst and have a small activation energy of 0.5 eV [115]. Na et al. proposed a single-step reverse precipitation preparation technique to control the physicochemical properties of nano-sized CeO_2 as support for low-temperature WGS reaction (Fig. 8e), which resulted in a high surface area support of 162.8 m^2/g [109]. They compared the catalytic activity with a normal precipitation method synthesized CeO_2 by supporting 5 wt% Cu on both the supports. The results indicated that the one with the support prepared by reverse precipitation exhibited higher CO conversion than the CeO_2 prepared by normal precipitation method [109].

The ceria support morphology has a significant impact on the properties of the catalysts and can affect the catalytic dispersion, water dissociation, the metallic-base stability, and the metal particle size upon reduction during WGS reaction. In this regard, Yao et al. synthesized three different shape-controlled CeO_2 nanostructured supports with CuO to catalyze WGSR [110]. The result showed that the nanospheres (NS) ceria support (Fig. 8f, g) had the highest activity and long-term stability in comparison to the nanorods (NR) and nanocubes (NC) [110].

Cámara et al. studied the effect of a novel manganese-doped inverse CeO_2/CuO catalyst under WGS reaction conditions [116]. The presence of Mn along with Cu strongly influenced the physical and chemical properties of the ceria nanoparticles leading to high catalytic activity towards WGS reaction [116]. They also examined CeO_2/CuO, Mn-doped CuO, and Zn-doped CuO for WGS catalytic performance, and the effect of O_2 and/or H_2 present in the reaction mixture. The result of this work demonstrated a positive impact of Mn and Zn doping on WGS performance; whereas for the undoped catalyst, CO conversion enhancement was seen in the presence of some oxygen at low temperature and high CO/O_2 ratio [117].

Tabakova et al. conducted a study aiming to introduce an efficient, cost-effective catalyst of alumina-supported Cu-Mn mixed oxides (Fig. 9a, b) synthesized by wet impregnation, where Au nanoparticles promoters were prepared by the deposition-precipitation approach [118]. According to the

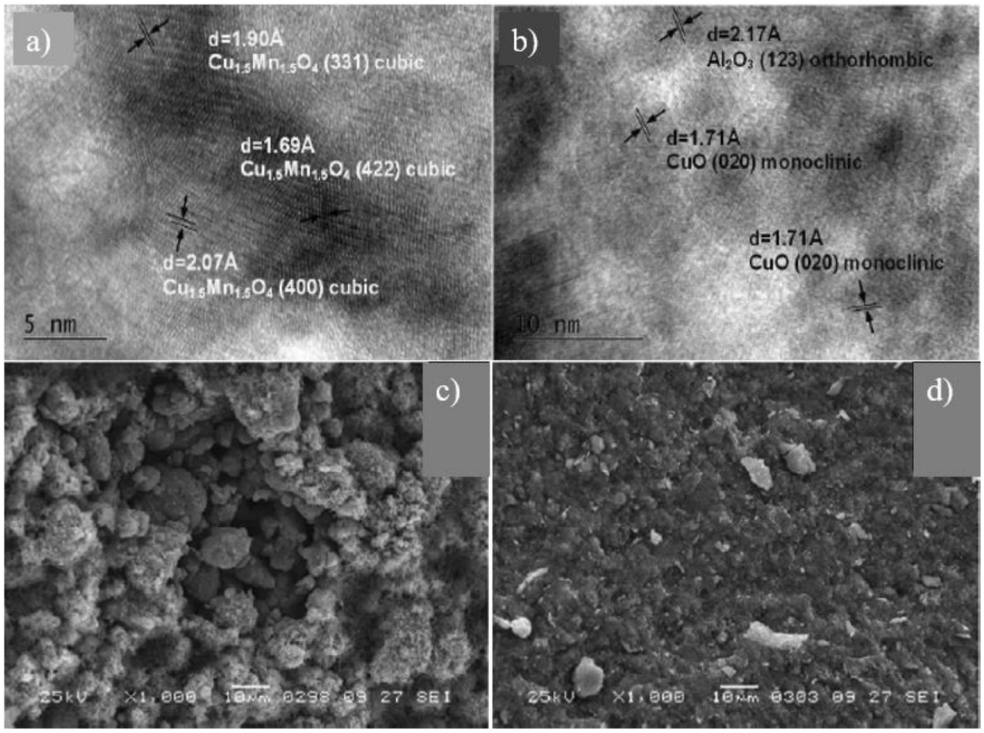

Fig. 9 **a**, **b** HRTEM micrograph of a fresh Au/CuMn (2:1) catalyst [117]. SEM images of **c** CuAl ceramometal and **d** CZA oxide catalyst [124]

result, the Au promotional effect was more demonstrated in a sample with a higher amount of Cu (Cu:Mn molar ratio of 2:1) due to the active presence of the two dispersed metallic phases. The high surface area of alumina modified by Cu-Mn mixed oxides surface fraction also favored the stabilization of dispersed gold nanoparticles. The high activity of this catalyst system makes it capable of practical usages, primarily due to economic viability as it consists of 80% alumina [118]. Sagata et al. investigated the effect of aluminum oxide and the pore size of the support on the catalytic activity during the low-temperature WGS reaction over Cu catalyst [119]. They concluded that by decreasing the mesopore size of Cu/Al_2O_3, the catalytic activity increased only when the steam/carbon (S/C) ratio was 2.2, whereas the catalytic activity increased in the S/C ratio of 4.6 by increasing the mesopore size [119]. One of the important considerations in an industrial sulfur tolerant WGS process is that the reaction conditions, not only catalysts, dictate many of the outcomes such as improvements in production capacity, decreasing production costs, and change in the catalytic activity [120, 121]. For example, Liu et al. developed Mo-Co/alkali/Al_2O_3 for sulfur tolerant WGS reaction that resulted in a steady operation even at 0.2–0.3 steam to gas ratio. Plant efficiency improvement, enhanced safety, and reduction in steam consumption during H_2 production were some of the key achievements [122].

Nano-structural composites of ceramometals (or cermets) can be attractive owing to reported catalytic property improvements compared to the common solid oxide supports. The ceramometals have excellent thermal conductivity and high strength as well as regulated mesoporous structure suitable for catalytic reactions to take place without much transport limitations [123]. Tikhov et al. synthesized porous CuAlO/CuAl ceramometals and tested for WGS reaction, where they reported the granulated ceramometals catalytic activity to be comparable with granulated CuZnAl oxide, owing to a high diffusion permeability (Fig. 9d) [124]. In another study based on low-temperature WGS, they compared catalysts prepared by co-precipitation method and ceramometal CuAlO/CuAl catalysts that were made from CuAl alloy powder (Fig. 9c). The catalysts activity was tested at one bar, using a mixture of CO: H_2O:H_2 = 8:42:50 and at a steam/gas proportion of 0.6–0.7 in both small (0.14–0.25 mm) and large (3.2 × 3.2 × 5 mm) portions. The result accordingly showed that the large fraction ceramometal catalyst had doubled the efficiency owing to a greater inner dissemination [125].

Longlong et al. studied the aluminum doping effect in Cu/ZnO/Al_2O_3 complex synthesized via modified co-precipitation method. The catalyst produced with this method containing 2.5% co-precipitated Al^{3+} of total Cu and Zn atoms exhibited higher activity and stability in the WGS reaction compared to the commercial sample [126].

Silva et al. studied the impact of H_2S on the platinum catalysts performance in WGS reaction. In this regard, they tested Pt-based catalysts with various oxides supports under real conditions, both with and without the presence of H_2S, thereafter extended the experiment further in the absence of H_2S to see if the catalyst performance can be recovered [127]. They found that zirconia incorporation to CeO_2 showed increased

sulfur tolerance as well as preserved high activity. They concluded that in the presence of H_2S, the $Pt/Ce_{0.25}Zr_{0.75}O_2$ showed the best performance in terms of lower deactivation, higher activity, and complete recovery, whereas under contaminated conditions, Pt/CeO_2 was not suitable anymore because of a higher deactivation rate [127].

Some reports indicate that the reducible oxides and solids providing oxygen vacancies can enhance the employed metal activity for the WGS reaction [128]. For example, García-Moncada et al. presented a multicomponent catalyst designed using different active phases (Cu, Pt, or Au) and different ionic conductors for WGS reaction [129]. The results of the study demonstrated that the ionic conductor, along with an appropriate catalyst, is necessary to the water supply as it potentiates activation of water as well as overall performance. The influence trend of ZrEu > MoEu > NbEu was observed for the ionic conductors, no matter the nature of the catalyst (Fig. 10a–c). The ZrEu ion was the most suitable conductor for the WGS reaction owing to the more oxygen vacancies provided by having a sub-stoichiometric structure [129]. A similar result was also presented by González-Castaño et al. in 2017 by using a bi-doped of Zr and Fe [130]. Yun and Guliants synthesized ZrO_2-supported Mo sulfide (Mo-S/ZrO_2) WGS catalysts using incipient wetness impregnation approach with different MoO_3 surface coverage (Fig. 10d–f). The CO conversion in WGS reaction over these catalysts increased with the presence of Mo content up to the monolayer coverage that showed a good correlation with the Mo sulfidation extent [131].

Molybdenum (Mo) and Molybdenum oxide (MoO_x) as promoters are reported to improve the performance of Pt-based WGS reaction catalysts (Fig. 11a) [132]. Pt-Mo/SiO_2 prepared with the impregnation-reduction technique have been used as effective catalysts in low-temperature (below 300 °C) WGS reaction. Pt nanoparticles with Mo promotion showed higher activity than Pt/SiO_2 due to an improvement in Pt dispersion as well as a synergistic effect in Pt-Mo system that were found to correlate with the atomic ratio of Mo/Pt (Fig. 11b) [132]. Marras et al. used two different types of porous silica, namely aerogel and cubic mesostructured, as supports for Cu-based nanoparticles that were tested for WGS reaction at 200–350 °C [133]. The catalytic performance was found to be influenced by the ability of the support matrices to disperse the copper nanoparticles. The results showed that the silica aerogel was a highly stable matrix throughout the catalytic cycles with a constant CO conversion [133].

TiO_2 is considered a good choice for catalyst support on the basis of as low-cost, non-toxic, and chemically stable nature. Some supports such as CeO_2 with variable oxidation states tend to be more effective only under specific conditions [134]. During the low-temperature WGSR, some metals,

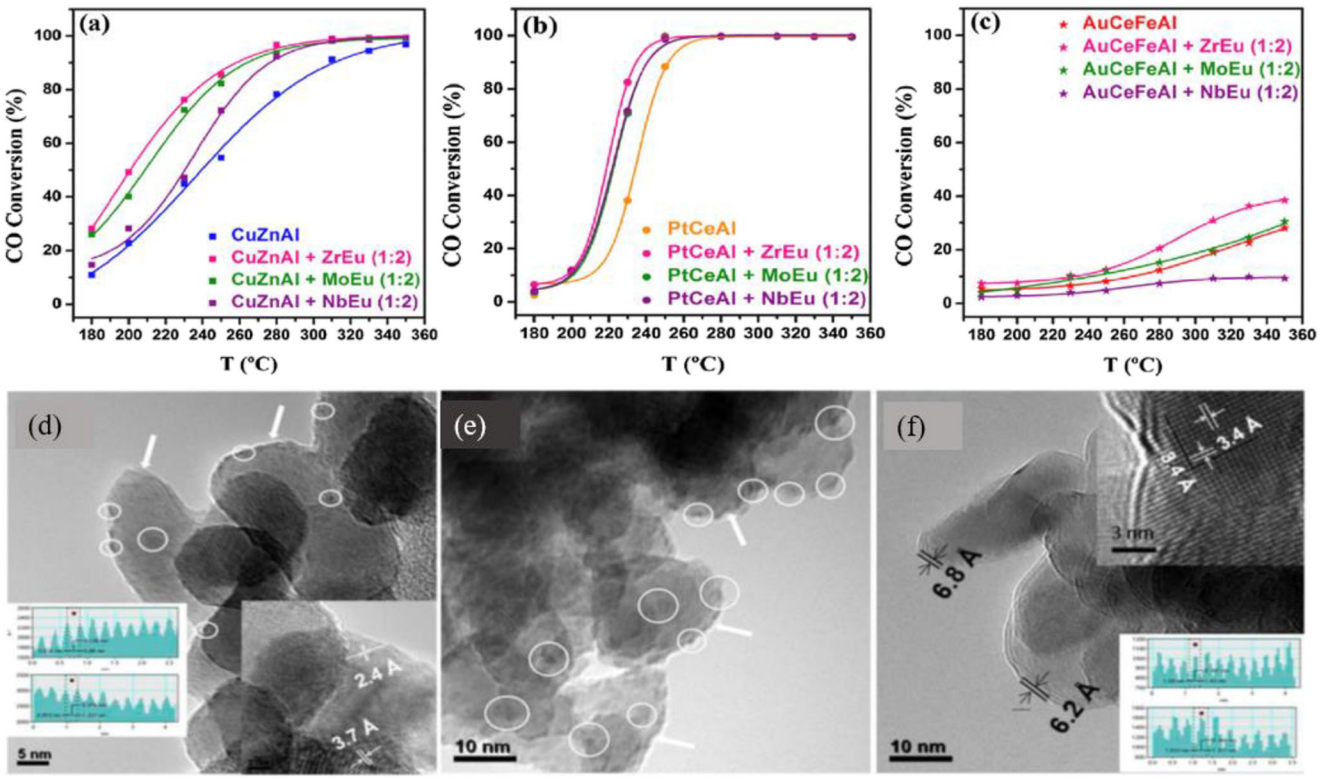

Fig. 10 **a**–**c** Temperature dependence of the CO conversion over **a** CuZnAl, **b** PtCeAl, and **c** AuCeAl; bare catalyst' activity and their mixtures with different ionic conductors. **d**–**f** TEM images of ZrO2 supported **d** Mo2-S, **e** Mo5-S, and **f** Mo15-S [130]

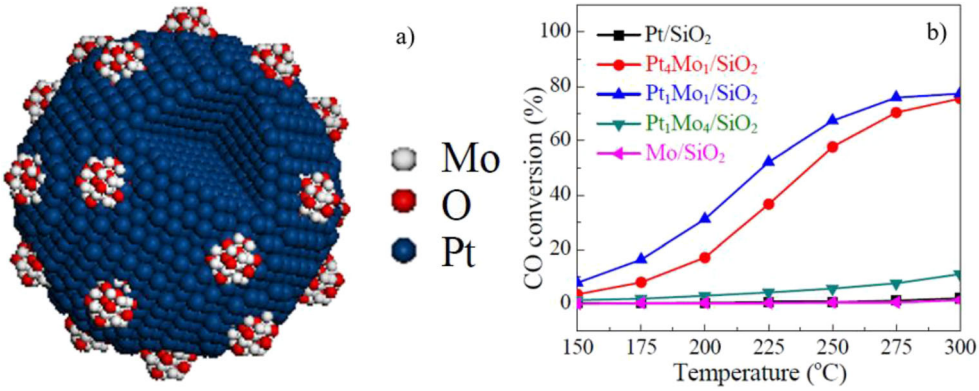

Fig. 11 **a** Schematic of Pt nanoparticles along with MoO_x nano-patches. **b** Temperature dependence of the CO conversion over different catalysts and Mo/Pt atomic ratios [131]

e.g., gold nanoparticles, tend to agglomerate even on rigid support like TiO_2 which has a higher ability to disperse them; nonetheless, this effect is reported to depend on the catalyst synthesis method as well [135]. For example, in a study conducted by Pérez et al., Au/TiO_2 was synthesized by different methods and Au loading was also controlled by three methods (double impregnation method (DIM), deposition-precipitation (DP), and liquid phase reductive deposition (LPRD)). The catalysts were evaluated for low-temperature WGSR and compared with the commercial sample provided by the World Gold Council (WGC) (Fig. 12a). The results revealed that the Au/ TiO_2 synthesized by the DP (Fig. 12b) method with 2.36% Au showed 85% CO conversion at 300 °C, while the WGC sample had just about 52% CO conversion under the same conditions [135]. Li et al. synthesized mesoporous, nanocrystalline composite catalysts of K/Pd/TiO_2 with different Pd molar ratio and tested their catalytic activity towards the low-temperature WGS reaction [136]. All the samples showed almost zero methane formation, whereas the inclusion of K in Pd caused a reduction in sintering, and supporting the Pd on smaller TiO_2 particle size resulted in better catalytic performance [136].

Apart from the well-known oxides, such as Al_2O_3, SiO_2, ZrO_2, CeO_2, and TiO_2, manganese oxides have also been reported as supports for low-temperature WGS reaction. The role of oxygen vacancies in manganese oxides has been critical, effective, economically favorable, and in some cases competitive to CeO_2 [137]. In this regard, Shan et al. reported a relatively good catalytic activity of Pd and Pt nanoparticles supported on α-MnO_2 nanorods (termed as Pd/α-MnO_2 and Pt/α-MnO_2) prepared by precipitation deposition method at 300 °C for WGSR with low-temperature (140–350 °C), which

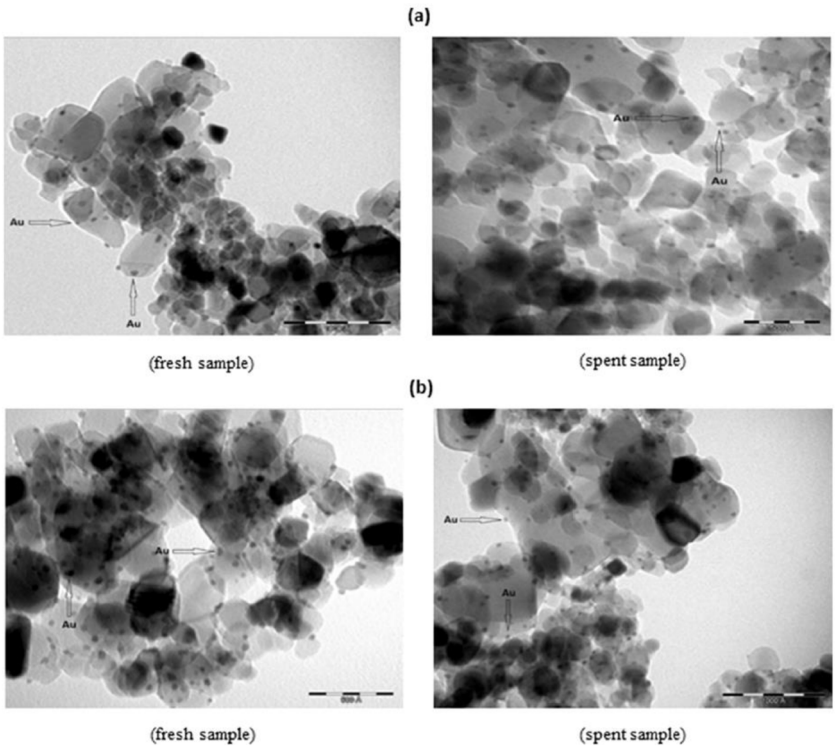

Fig. 12 HRTEM images for both fresh and spent Au/TiO_2 catalysts: **a** WGC, **b** DP-2.36% [135]

were comparable to Pd/CeO_2 and Pt/CeO_2. The surface oxygen vacancies density of the catalysts generally remained at 10–15% during the WGS reaction [137]. Poggio-Fraccari et al. evaluated copper and nickel separately as monometallic catalysts supported on cerium-manganese mixed oxides through a WGS reaction, where they found that both Cu and Ni performed best on MnO_x-CeO_2 oxides support with 30% Mn:Ce molar ratio [138]. Pd/CeO_2 catalysts are believed to show irreversible deactivation in the WGS reaction owing to losses in the metal surface area. Some reports suggest the use of transition metals as additives in Pd/CeO_2 to counter the irreversible deactivation [139]. Xiao et al. tested $PdO/MnO_x/CeO_2$-ZrO_2 catalyst along with a series of other catalysts as references (e.g., PdO/CeO_2-ZrO_2, PdO/Al_2O_3, $PdO/MnO_x/Al_2O_3$, CeO_2-ZrO_2, and MnO_x/CeO_2-ZrO_2) [140]. They reported an enhancement in the WGS activity by using manganese oxide, which possibly could be due to an improvement in the redox property in presence of Pd-Mn and particularly Mn-Ce interactions. The other reason for catalytic performance enhancement was attributed to the formation of metallic Pd species because of the electron-donating effect of MnO_x neighbor, which facilitates water dissociation [140]. Lanthanum is also reported to have a unique electronic structure and oxygen storage capability to act as co-catalysts, where it can store as well as release oxygen during oxidation-reduction reactions. In a study conducted by Runxia et al., the effects of La loading on Cu-Mn catalysts towards low-temperature WGS reaction were investigated, and the results showed significant improvement in the catalyst activity by using 0.5 mol% La [141]. The introduction of La resulted in an increase in the dispersion of Cu on the catalyst surface, as well as a more uniform distribution of Cu and Mn in the catalyst [141].

2.4 Carbon-based supports

Carbon, in different forms, has gained significant research interest as a support for active sites in catalysis [142]. An investigation, by Zugic et al., on Pt supported on oxygenated multi-walled carbon nanotubes (MWNTs) indicates that platinum can be activated by controlled addition of alkali promotor (Na) on MWCNTs (Fig. 13a) [143]. Pt on MWCNs without Na was however reported to be not active for the WGS reaction. The sample prepared by suspending MWNTs (C_N) in the HNO_3 solution for 2 h and then dissolving in 1 M sodium acetate with a heat-treatment at 800 °C (Pt/800-Na-2hr-C_N; Fig. 13b, c) was found to have the highest WGS activity (Fig. 13d) [143]. In another study, they also reported a direct promotional impact of sodium on the WGS platinum activity and stability when supported on oxygen-free C_N. The co-impregnation of 1 wt% Pt and Na on the annealed nanotubes (1 wt% Pt_1Na_6/1000-2h-C_N; Fig. 13e, f) resulted in an exceptionally high catalytic activity in WGSR [144].

Dongil et al. examined two commercial Ni/CeO_2/CNT catalysts for low-temperature WGSR; moreover, they also used activated carbon for comparison [145]. They demonstrated that CNTs improved the dispersion of ceria, leading to a better CO activity than the ceria used with activated carbon. Furthermore, in conditions where CO_2 and H_2 exist in the feed, the activity decreased slightly, and methanation was discovered at temperatures only above 573 K [145].

Carbon nanofibers (CNF) is another promising alternative to metal oxide-based supports due to the unique structural characteristics that enhance the metal and support interactions. They also have high mechanical strength, high electrical conductivity, and specific surface area, which is suitable for formation and anchoring of smaller metal nanoparticle [146]. Oliveira, Valençaa, and Vieira studied both Cu/CNF and Cu/Al_2O_3 catalysts for the WGS reaction at a temperature range of 398–573 K [147]. In the case of the lowest evaluated water partial pressure and H_2O:CO ratio of 3.1, Cu/CNF exhibited the highest activity. In the WGS reaction, however, 5% Cu/Al_2O_3 exhibited better results owing to the support hydrophobicity of Cu/CNF that prevents water adsorption [147].

Graphitic oxides are also reported to enhance the catalytic performance due to their surface chemical functions and confinement effects [149]. Dongil et al. successfully investigated the low-temperature WGS reaction using both binary Ni/Graphene and ternary Ni-CeO_2/graphene systems with 5 wt% Ni and 20 wt% CeO_2 and compared them with $NiCeO_2$ catalyst [148]. The catalytic activity improved with sodium addition in the presence of Ce (Ni-CeO_2/G-Na), possibly due to the promotional effect of Na in facilitating ceria reduction (Fig. 14) [148]. Pastor-Perez, Buitrago-Sierra, and Sepulveda-Escribano dispersed different loadings of cerium oxide over activated carbon and investigated their catalytic behavior [150]. The synthesis resulted in small ceria particles, high surface area, and an easier reduction of ceria in the presence of Ni. The catalysts, Ni supported on different loading of CeO_2/C as well as Ni/CeO_2 (Fig. 15a) were examined for the low-temperature WGSR. The optimum amount of CeO_2 loading was determined to be 20 wt% (Fig. 15b); however, in the realistic conditions, in the presence of CO_2, the catalyst with 10 wt% CeO_2 showed a better performance. The $Ni10CeO_2$/C catalyst was found to have a 40% CO conversion after a 150-h stability test at 493 K (Fig. 15c, d) [150]. In a comparative study conducted by Pastor-Pérez et al. on the WGS performance using Ni/CeO_2 bulk and $Ni20CeO_2$/C, the carbon-supported catalyst showed far more activity than the one without the carbon support which can be due to its capacity to store oxygen. Moreover, the Ni-CeO_2/C stability (Fig. 15e, f) was evaluated under practical conditions, revealing a considerable catalyst activity loss, owing to the Ni particles sintering [151].

A summary table is provided below to enlist the different catalysts used in the review. The synthesis methods and

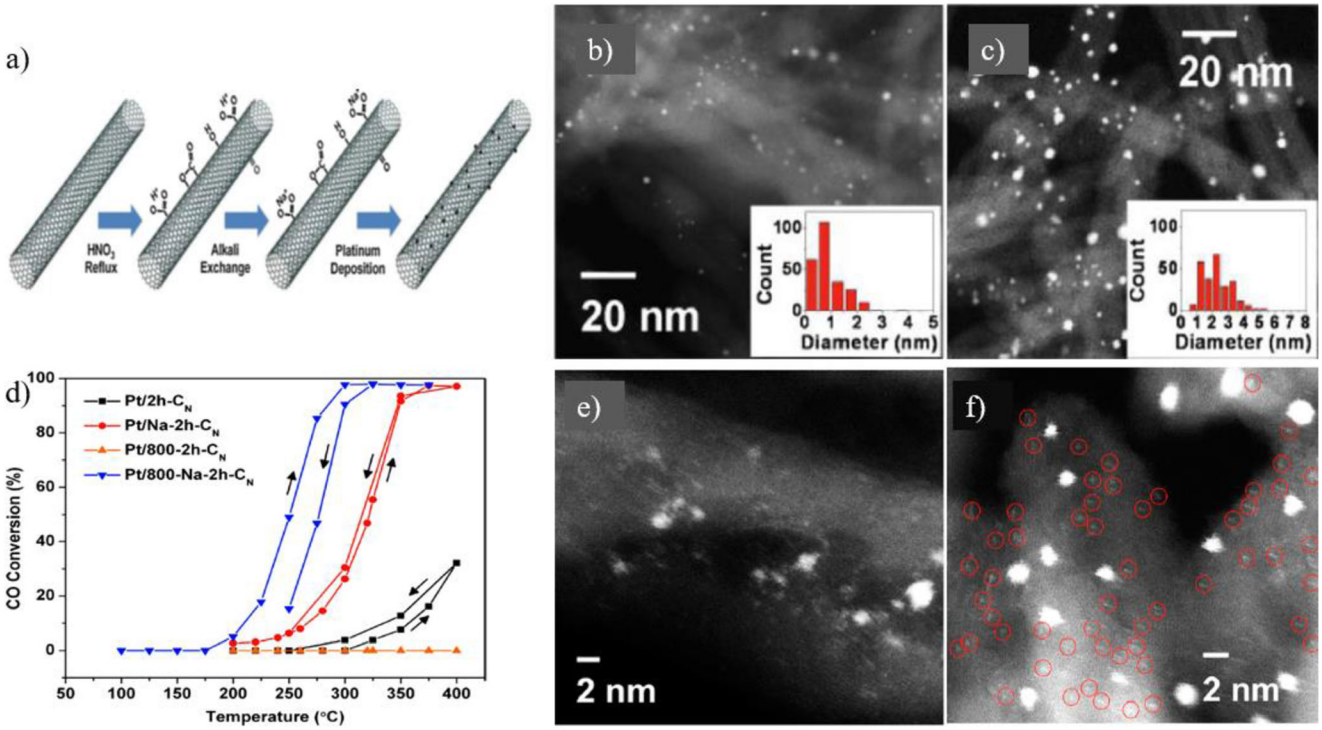

Fig. 13 **a** Preparation schematic of alkali-promoted Pt/MWNT catalysts. **b**, **c** HAADF-STEM images of **b** fresh Pt/800-2h-C_N and **c** used Pt/800-2h-C_N. **d** Temperature dependence of the CO conversion over Pt catalysts on different supports [143]. **e**, **f** HAADF-STEM images of **e** fresh Pt_1Na_6/1000-2h-C_N and **f** used Pt_1Na_6/1000-2h-C_N (red circles are atomically scattered species) [144]

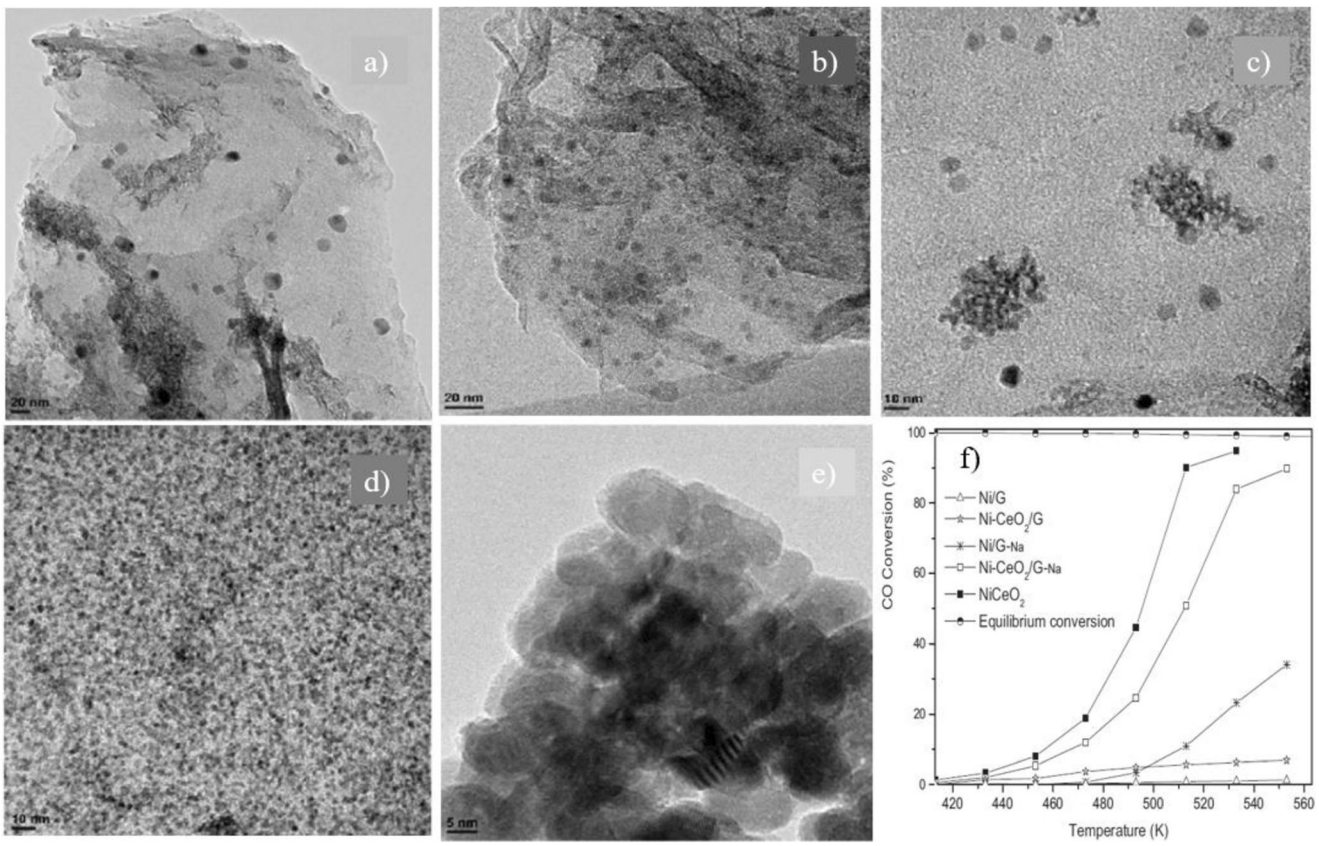

Fig. 14 **a**–**e** TEM micrographs of **a** Ni/G-Na, **b** Ni/G, **c** Ni-CeO_2/G, **d** Ni-CeO_2/G-Na, **e** $NiCeO_2$, and **f** temperature dependence of the CO conversion over different catalysts [147]

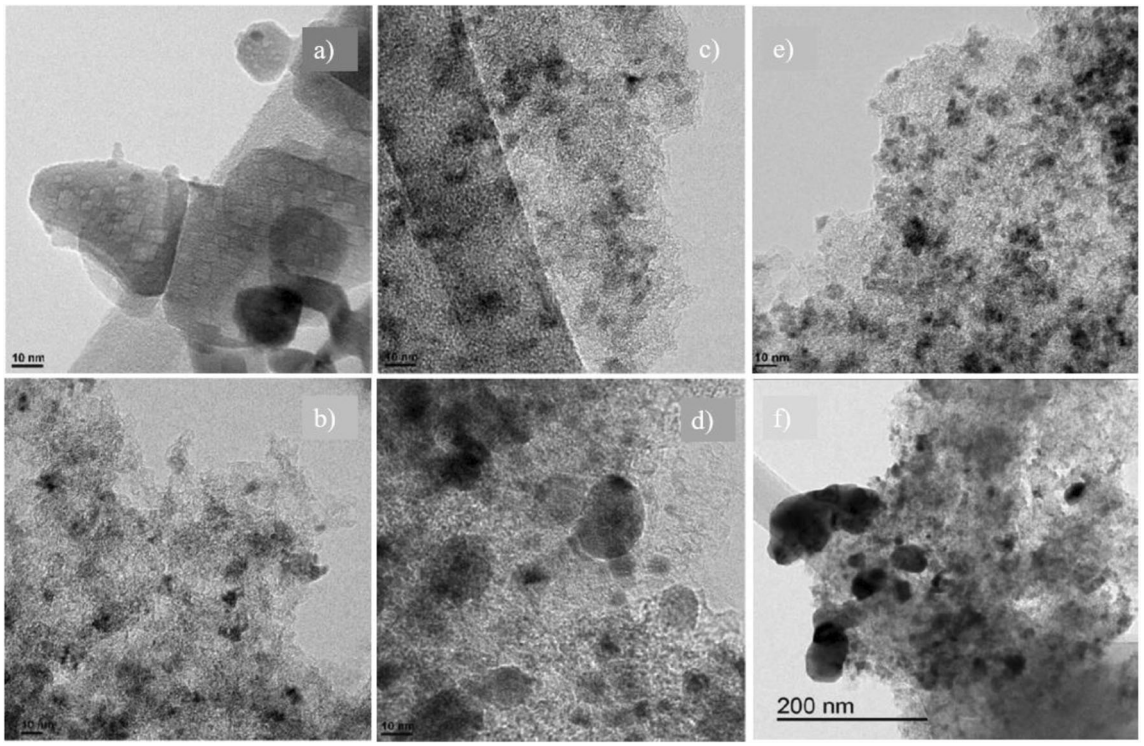

Fig. 15 **a**, **b** TEM micrographs of **a** Ni/CeO_2, **b** Ni20CeO_2. **c**, **d** TEM micrographs of the Ni10CeO_2/C catalyst **c** before and **d** after the stability reaction test at 220 °C [149]. **e**, **f** TEM micrographs of the Ni-CeO2/C catalyst **e** before and **f** after the stability reaction test at 250 °C [150]

experimental conditions under which the catalysts were evaluated for WGS reaction are also provided along with the key results in a convenient way to compare their performance (Table 1).

To understand the effect of nanostructure and shape of active metals at nanoscale, following table is constructed by coming the literature reports on similar materials with different nanostructures and morphology (Table 2).

2.5 Summary and future outlook

WGSR is one of the commonly used industrial reactions for hydrogen production, and by some estimates, approximately 10% of the annual world energy consumption by 2030 will be linked to the WGS reaction [153]. The WGSR is a well-established procedure in conventional chemical/hydrocarbon industries for the production of ammonia, methanol, hydrogen, saturated hydrocarbons, and many other chemicals and petrochemicals. Thermodynamically, WGSR should be conducted at low temperatures for higher hydrogen selectivity; however, low temperature reduces the kinetics rate and thereby increases the required amount of catalysts to achieve high CO conversions [154]. The recent few years have seen considerable growth in nanomaterials and chemical characterization techniques, leading to unique details that were unheard of before. The catalysis community has benefitted significantly with these developments in understanding the dynamic changes in the structure of the catalysts in situ during the reaction conditions, in a more realistic environment than under ultra-high vacuum. Herein, we provided a review of the recent development in the catalysts used for low-temperature WGSR focusing on the nanostructure of the catalysts along with other key factors influencing catalytic performance, such as synthesis technique, nature of active site/phase and support, and reaction environment.

Introducing support materials, especially those with controlled and uniform nanostructured morphology, onto various metal, non-metal, and carbon-based catalysts can be beneficial in achieving catalytic systems with larger surface area and abundant active sites resulting in higher CO conversion activity, and long-term stability. Supports with oxygen storage capacity, such as CeO_2, are particularly favorable for low-temperature WGSR. Synergistic effects of combining different catalysts or adding various alkali promoters not only improve the performance of the existing catalysts but also help in reducing the overall cost by introducing earth-abundant elements in developing new types of highly active and stable catalysts. Notably, the introduction of promoters leads to a high chemical and thermal stability for these catalysts by limiting the sintering of smaller particles under severe reaction conditions. Many of the recent work focused on single-atom catalysis to achieve a very high dispersion of the active sites encapsulated on the support structure, which seems to achieve higher turnover rates compared to bigger nanoparticles.

Table 1 A summary of catalysts, synthesis method, experimental conditions, and key results

Catalyst	Synthesized method	Experimental condition	Result	Ref
Pt-based				
Pt/CeO_2 Pt/CeGa (Ce80Ga20)	Pt: incipient wetness impregnation CeO_2: direct precipitation CeGa: precipitation with ammonium hydroxide (direct co-precipitation or inverse co-precipitation)	Fixed bed stainless steel tubular reactor -50 mg catalyst diluted with 100 mg quartz -Feed composition: 1% CO, 2% H_2O balanced with He -Total flow: 100 cm^3 min^{-1}	-Feasibility of tuning the support vacancies by doping ceria with gallium (while metal dispersion will stay constant). -Fast oxygen vacancy filling by water in either Pt/CeO_2 or Pt/CeGa -Higher activity of Pt/CeO_2 than Pt/Ce80Ga20	[31, 152]
Pt/CeO_2	Hydrothermal method (175 °C, 24 h)	Fixed bed downflow reactor -200 mg catalyst -Atmospheric pressure -Temperature: 50–200 °C -GHSV: 5000–40,000 h^{-1} -Feed: CO:H2O:He = 3:3:94 -Pt nanoparticles size: 0.8–8	-The0.9Pt-CeO_2 had the highest CO conversion (85.1%) and 1.66×10^{10} mol cm^{-1} s^{-1} CO formation rate at 140 °C. -The catalytic activity decreases with increasing Pt loading.	[32]
$Pt/M/CeZrO_4$ (M = Na, Mo, Sn, Cu, Zn)	Wet impregnation	Fixed bed tubular stainless steel reactor -Atmospheric pressure -Feed: 8% CO, 30% H_2O, nitrogen balance -Flow rate of 1000 Ncm^3/min -GHSV: 10,000 h^{-1} -Temperature: 423–673 k	The performance of Pt-based catalysts could be enhanced by employing another metal for alloy formation.	[38]
Pt-CeO_x/Al_2O_3	Supercritical fluid deposition Deposition of ceria onto γ-alumina: incipient wetness impregnation	OD quartz tube reactor -Feed: 16%/32%/32%/20% $CO/H_2/H_2O/N_2$ -Total gas flow rate: 250 SCCM -GHSV:75,000 mL g^{-1} h^{-1} -Catalyst pellets size: 500 μm -Amount of catalyst in the reactor: 200 mg -Temperatures: 250–450 °C	-No methane formation or carbon deposition -The supercritical fluid deposition application as a scalable technique for noble metal catalyst preparation	[39]
KOH-coated Pt/Al_2O_3 ($KOH/Pt/Al_2O_3$)	Commercially purchase of Pt/Al_2O_3 then immersed into KOH solution	Catalyst bed -Feed: 10% H2O and 11% CO in Ar -Total flow:4 $mL_N min^{-1}$ -Pressure: atmospheric	-H_2 production starts at temperatures around 160 °C -Increase activity by KOH additive -64% selectivity of the coated catalyst at whole range of temperature -Positive effects on both WGS and MSR reactions by using the KOH cheap coating	[40]
$Pt/CeO_2/Al_2O_3$	Pt (2 wt%) deposited by wet impregnation on commercial $20CeO_2$–$80Al_2O_3$ then calcined at 350 °C for 8 h at heating rate of 5 °C/min (buffer layer: CeO_2-Al_2O_3, catalyst layer: Pt (2%)/CeO_2-Al_2O_3 supported on the buffer)	Tubular flow reactor -Feed (model condition): 4.5% CO, 30% H_2O, and 66.5% N_2 (Real condition): out-gas feed stream reformation containing 7% CO, 9% CO_2, 50% H_2, and 30% H_2O balanced with N_2 -Total flow: 400 ml min^{-1} -Pressure: atmospheric -Temperature: 180–350 °C -GHSV = 4000 h^{-1}	-In real condition, buffer layer enhances the catalytic activity. -Buffer layer has capacity for water dissociation under reductive atmospheres.	[41]
Pt-Re/Ti	Pt and Re clusters deposition onto a rutile crystal of TiO_2 (110)	Ultra-high vacuum chambers -Feed: 3% CO/7% H_2O/90% He	-Greater activity with the bimetallic catalyst than pure Pt clusters.	[42]

Table 1 (continued)

Catalyst	Synthesized method	Experimental condition	Result	Ref
	-Heating the sample to 130–190 °C at a rate of around 1.5–2 °C/min before reaction	-Flow rate: 60 SCCM -Temperature: 130–190 °C	-Lower activity of pre-oxidized Pt-Re clusters than the unoxidized Pt-Re one.	
Pt/MoC Pt/TiC (001)	Pt vapor deposition on the surfaces of TiC (001), polycrystalline δ-MoC, and β-Mo_2C (001) at 300 K.	Micro-reactor -Feed: CO (20 Torr) and H_2O (10 Torr)	-Small Pt coverages on the carbide substrates has the highest catalytic activities -The metal/carbon ratio has a strong effect in the stability and selectivity. -No methane formation over Pt/MoC and Pt/TiC.	[43]
Pt/TiO_2	Reverse micelles -Pt nanoparticle tunable size: ~ 1.0 to ~ 2.6 nm. -Ti nano shells: ~ 32 nm diameter and ~ 3–5 nm thickness.	Fixed bed quartz tubular reactor -Feed: He/CO/H_2O = 88/2/10 volume ratio. -Flow rate: 15 mL min^{-1}	-By decreasing Pt nanoparticles size, stability, and activity enhance.	[33]
$Pt/Mo_2C/Al_2O_3$	Wet impregnation (both for support and promoter preparation) -The catalyst pretreated with 15% CH_4/H_2 and 100 mL min^{-1} flow rate at 590 °C for 2 h with 10 °C min^{-1} heating rate.	Fixed bed reactor -Feed: 11% CO, 43% H_2, 6% CO_2, 21% H_2O, and balance He -Temperature: 180–300 °C -GHSV: 125,000 h^{-1} -Catalyst amount: 100 mg -Fraction size: 250–425 μm	-Different acidic supports such as η-Al_2O_3 and γ-Al_2O_3 can let to different interaction and synergetic among the two most active Pt metal and Mo_2C phases. -4 Pt-Mo2C has the highest activity and stability (over 85 h at 250 °C)	[34]
$Mn_{2.94}M_{0.06}O_{4-\delta}$ (M = Pt, Ru, Pd)	Sonochemical -Room temperature -Catalyst particles: 60/80 mesh size)used without reduction(	Quartz reactor -Catalyst amount: 100 mg -Feed: 2% CO and 98% N_2 -Pressure: atmospheric -GHSV: 48000 h^{-1} -Flow rate: 100 mL min^{-1}	-At 260 °C $Mn_{2.94}Pt_{0.06}O_{4-\delta}$ catalyst had the highest conversion of 99.9% with methane formation due to a strong interaction existing between Pt and Mn_3O_4	[35]
Pt/FeO_x	Co-precipitation -Catalyst size: nanoparticles and single atoms -Catalyst reduction: at 300 °C with 20 mL min^{-1} flow of 10 vol% H_2/He.	Fixed bed reactor -Pressure: atmospheric -Catalyst amount: 100 mg -Feed: 2 vol% CO + 10 vol% H_2O + He -Flow rate of 30 mL min^{-1} -GHSV: 18000 mL g_{cat}^{-1} h^{-1}	-Reaction mechanism changes with Pt dispersion increase. -Reaction rates and turnover frequency increase with reducing Pt species size from nano to single atoms	[36]
Pd-based				
$Pd/K/Co_3O_4$	Impregnation and physical mixture Catalyst size: 250–500 μm	Fixed bed flow reactor -Pressure: atmospheric -Catalyst amount: 40 or 80 mg -Feed: H_2O:CO:H_2:N2: Ar, 30:6:42:13:9 -Flow rate = 178 mL min^{-1} -Reaction temperature: 573 K	-Catalyst prepared by impregnation method had higher initial activity compared to the physical mixture -The presence of K in the catalyst affected the CO adsorption species resulted in high activity	[48]
Pd/FeO_x (Pd/Al_2O_3 as reference)	Co-precipitation -Pretreated with 10 vol% H_2/He in a flow rate of 20 ml min^{-1} at 300 °C for 30 min and purging with He for 1 h	Continuous flow fixed Bed reactor -Catalyst amount: 100 mg -Pressure: atmospheric -Feed: 2 vol% CO, 10 vol%H_2O, and balanced with He -WHSV: 18000 ml h^{-1} g_{cat}^{-1}	-The FeO_x facilitated the higher Pd dispersion than Al_2O_3 -Higher CO conversion and good stability of Pd/FeO_x than Pd/Al_2O_3 even with CO_2 and H_2	[47]
Au-based				
	-Support: incipient	Tubular flow reactor		[51]

Table 1 (continued)

Catalyst	Synthesized method	Experimental condition	Result	Ref
$Au/(CeO_2/Al_2O_3$ and $Ce_{0.8}Fe_{0.2}/Al_2O_3$ $Pt/(CeO_2/Al_2O_3$ and $Ce_{0.8}Fe_{0.2}/Al_2O_3$	wetness impregnation -Au-based catalysts: direct anionic exchange and with no pretreatment -Pt-based catalysts: aqueous impregnation with an activation process of 2 h at 350 °C in a 10 vol% H_2 stream	-Pressure: atmospheric -Catalyst amount: 1 g -Temperature: 180–350 °C -Feed: in model condition only H_2O (31.1 KPa) and CO (4.5 vol%) diluted in N_2 (balance), in real conditions H_2O (31.1 KPa), CO (9 vol%), H_2 (50 vol%) and CO_2 (11 vol%) -GHSV: 4000 h^{-1} -Bed volume: 1.5 cm^3	-The presence of Ce or mixed CeFe oxide were in favor of the WGS activity for both Au or Pt -The higher the sample bandgap, the higher the catalytic activity -Au-based catalysts more affected by the support's electronic properties than Pt-based -Regardless of stream composition, the Au-based catalysts perform better activity than the Pt ones at 180 °C	
Au/Ceria-iron mixed oxide Pt-Ceria-iron mixed oxide	-Support: impregnation -Au-based catalysts: direct anionic exchange and with no pretreatment -Pt-based catalysts: aqueous impregnation with an activation process of 2 h at 350 °C in a 10 vol% H_2 stream	Tubular fixed bed reactor -Pressure: atmospheric -GHSV: 4000 h^{-1} -Feed: in classical mixture 4.5 vol% CO and 30% H_2O balanced in N_2, in the O_2-assisted WGS 0.7 vol% O2+ 4.5% CO + 30% H_2O balanced in N_2 -Bed volume: 1.5 cm^3	-In the conventional condition Pt is the most active metal while in the O_2 assisted WGS, Au-based has better performance. -Adding O_2 to the WGS feed stream promotes the WGS catalytic activity, significantly for Au and slightly for Pt-based catalyst.	[52]
Au/Fe_2O_3	-Deposition-precipitation (DP) -Liquid phase reductive deposition (LPRD) -Double impregnation method (DIM) (the catalysts preheated and reduce before testing)	Fixed bed reactor -Catalyst amount: 0.2 g -Feed: 4.7 vol% CO, 10.1 vol% CO_2, 35.4 vol% H_2O and 28.5 vol% H_2, balanced with N_2 -Pressure: atmospheric -Temperatures: 150–300 °C -Flow rate: 50 ml_N/min	-Au improves the Fe_2O_3 support reducibility and it is highly dispersed on this support. -The highest CO conversion was belonged to the catalyst with DP preparation method.	[53]
$Au/Ce_{1-x}Cu_xO_2/Al_2O_3$	-Support: co-impregnation -Gold deposition: direct anionic exchange assisted by NH_3 -Catalyst particle size: 600–800 μm	Tubular flow reactor -Pressure: atmospheric -Temperature: 140–350 °C -Bed volume: 1.5 cm^3 -GHSV: 4000 h^{-1} -Feed: 30 vol% H_2O + 4.5 vol% CO balance in N_2	-Although Cu is considered an active phase in the WGS, the presence of Au is important to obtain high performance -The materials' properties are considerably affected by the Ce/Cu ratio -Ceria has a crucial role in achieving optimum performance and more excellent stability.	[55]
$Au-Re/CeO_2$	-Ce support: deposition-precipitation (DP) -Au/ceria catalysts: deposition-precipitation (DP) or homogeneous deposition-precipitation (HDP) -Au-Re/ceria catalysts: sequential HDP (catalysts reduction at 300 °C for 1 h with 100 ml min^{-1} of pure H_2	Fixed bed reactor -Pressure: atmospheric -Temperature: 200–400 °C -Flow rate: 100 cm^3/min -Catalyst amount: 250 g	-The monolithic catalyst synthesized by the HDP approach had superior performance than the DP technique. -The presence of Re as a promoter and modifying the HDP method made CO conversion over the monolithic catalyst higher than the particulate ones. -The monolithic $Au-Re/CeO_2$ performance was determined to be promising for both ideal and realistic feed conditions.	[57]
Au/α-MoC	Precipitation followed by sequential temperature-programmed ammonization and carburization.	-Feed: (1) in product-free condition: 10.5% CO/21% H_2O/20% N_2 in Ar, (2) in full reformate condition: 11% CO/26% H_2O/26% H_2/7% CO_2 in N_2 -GHSV: 180000 h^{-1}	-At 393 K, α-MoC had 34% CO conversion under the product-free gas -The (2%) Au/ α-MoC catalyst exhibited above 95% conversion at 393 K and 98% at 423 K, above 523 K, CO conversion fell.	[54]

Table 1 (continued)

Catalyst	Synthesized method	Experimental condition	Result	Ref
$Au/Cu\text{-}ZnO\text{-}Al_2O_3$	-$Cu/ZnO/Al_2O_3$ support: conventional co-precipitation -Gold deposition: deposition-precipitation (DP) -Catalyst particle size: 600–800 μm	Tubular flow reactor -Pressure: atmospheric -Temperature: 160–350 °C -Feed: (1) in model condition: 4.5%CO, 30% H_2O and N_2 as balance, (2) in real conditions: 9% CO, 30% H_2O, 11% CO_2 and 50% H_2 -GHSV: 2000 and 4000 h^{-1}	-The hydrotalcite precursor made catalysts' microstructure homogeneous that ensures great Au and Cu dispersion and increased metal-oxide contact. -These materials overcome the major problems existing in commercial WGS catalysts	[59]
Au/CeO_2 (Au_Cluster & Au_Particle)	-Ceria nanorods: hydrothermal (at 100 °C for 24 h) -Au_Particle catalyst: colloidal deposition -Au_Cluster catalyst: deposition-precipitation -Catalyst size: 20–40 mesh -Catalyst pretreated: in air at 300 °C for 30 min then under WGS reactions (2% CO/12% H_2O in He, 30 ml/min) at 300 °C for 1 h	Fixed bed reactor -Pressure: atmospheric -Catalyst amount: 100 g -Feed: 2% CO/12% H_2O/N_2 -SV: 42000 ml h^{-1} g_{cat}^{-1} -Temperature: 100–350 °C	- Au_Cluster catalyst showed much better catalytic performance than Au_Particle in the WGS reaction.	[60]
$Au/Cu\text{-}ZnOAl_2O_3$	-$Cu/ZnO/Al_2O_3$ hydrotalcites: conventional co-precipitation -Gold deposition: deposition-precipitation -Catalyst particle size: 600–800 μm	Tubular flow reactor -Pressure: atmospheric -Temperature: 140–350 °C -Feed: (1) in model condition: 4.5%CO, 30% H_2O and N_2 as balance, (2) in real conditions: 9% CO, 30% H_2O, 11% CO_2 and 50% H_2 _GHSV: 2000 and 4000 h^{-1}	-Au-Cu synergy is an important parameter to optimize performance. -Using hydrotalcite type of precursor makes catalysts' microstructure homogeneous and increase the metal-oxide contact.	[62]
$Au/Ce_{1-x}Ti_xO_2$	-$Ce_{1-x}Ti_xO_2$ supports: sol-gel -Gold deposition: deposition-precipitation	Custom-made fixed bed flow reactor -Pressure: atmospheric -Temperature: 150 °C -Catalyst amount: 0.150 g -Feed: 2% CO, 2% CO_2, 7.5% H_2O, 8.1% H_2, and N_2 to balance -Flow rate: 100 ml min^{-1} -GHSV: 52000 h^{-1}	-The amorphous $Ce_{0.2}Ti_{0.8}O_2$ had the highest surface area. -The catalyst stability could improve with considering the necessary properties to obtain highly dispersed, well-anchored gold species	[65]
Rh-based				
Rh/TiO_2	Conventional deposition-precipitation -Catalyst reduction: 10 vol% H_2/He at 200 °C for 30 min with 20 mL min^{-1} flow rate	Continuous flow fixed bed quartz tubular reactor -Pressure: atmospheric -Catalyst amount: 100 mg -Feed: 2 vol% CO, 10 vol% H_2O and He mixture of 30 mL min^{-1} -WHSV: 18000 ml $h^{-1}g_{cat}^{-1}$ -Rh loadings: 0.01 to 2.5 wt (heating the gas lines 120 °C to prevent water condensation)	-0.4 wt% single atoms Rh_1/TiO_2 (CO/Rh = 1) catalyst had an enhanced CO conversion efficiency with high stability and without methanation side reaction.	[66]
Rh and Al co-doped ceria ($Ce_{0.93}Al_{0.05}Rh_{0.02}O_{2-\delta}$)	Single step solution combustion -Catalyst size: 150–300 μm	Quartz tube reactor -Catalyst loadings: 25 mg, 50 mg, 100 mg, and 200 mg -Flow rate: 100 mL min^{-1}	-The synthesized method made the catalyst porous with relatively high surface area.	[68]

Table 1 (continued)

Catalyst	Synthesized method	Experimental condition	Result	Ref
		-Feed: 2 vol% CO and H_2O		
Ru-based				
Ru-iongel (supported IL phase catalyst as reference)	The synthesized catalyst preheated in a CO/N2 atmosphere to 120 °C	Tubular fixed bed reactor -Catalyst amount: 0.4 g -Flow rate: 80 mL min^{-1} -Feed: 70% N_2, 20% H_2O, and 10% CO -Pressure: 0.3 MPa (The reaction firstly carried at 120 °C for around 40 h)	The iongel catalyst exhibited high activity at a temperature range of 120 to 160 °C. -The higher the IL loading is, the higher catalytic activity the iongal has. -The iongel with more anions has higher activity.	[71]
Ru/C	-Ru catalyst: impregnation -Activated carbon pretreated: 30 wt% HNO_3 at 90 °C for 4 h -Ru/C catalyst: impregnation (The catalyst reduced by three different material: $NaBH_4$, ethylene glycol, H_2)	Tubular fixed bed reactor -Catalyst amount: 0.4 g -Flow rate: 80 mL min^{-1} -Feed: 70% N_2, 20% H_2O and 10% CO -Pressure: 0.3 MPa -Temperature: 200 °C to 325 °C	-Adding K_2CO_3 is significantly improve both the activity and selectivity of the Ru/C catalyst.	[69]
Ru/C	2%Ru/C catalysts: impregnation	Fixed bed reactor -Temperature: 453–553 K -Feed: 11.36% CO, 22.72% H_2O, and 66.8% Ar	-80% of CO conversion was achieved at 553 K. -Finding the best preparation techniques or the experimental condition is the best way to enhance the catalytic performance	[72]
Ru/TiO_2 Ru/Al_2O_3	Wet incipient impregnation -Catalyst reduction: gas mixture of H_2, N_2, 0.025 L min^{-1} at 400 °C, for 3 h.	Tubular stainless steel reactor -Feed: 11% CO, 22.72% H_2O, and 66.28% Ar -Temperature: 453–573 K -Pressure: atmospheric	-Using water as a reactant positively affects the WGS process performed with Ru/Al_2O_3 catalyst. -No methane produced with using both catalysts	[73]
Ru/TiO_2	Wet impregnation -Catalyst particle size: 412 μm	Fixed bed membrane reactor -Pressure: atmospheric -Temperature: 453–575 K -Feed: $CO/H_2O/Ar$ -Reactants flow rate: 0.0015 h^{-1} -H_2O/CO feed ratio: 4:1 M -CO flow rate: 1.50×10^{-5} m^3 h^{-1} with 15% CO in Ar (the operation take place both with and without hydrogen permeation)	-At 573 K, with H_2 permeation, CO conversion and H_2 recovery were 90 and 76%, respectively. -Without H_2 permeation, the CO conversion was 26% higher than the amount with using hydrogen permeation, and the H_2 recovery was also five times higher.	[74]
Cu-based				
Mo/Co/K/ZSM-5 Mo/Ni/K/ZSM-5 (with and without Cu-based catalyst)	-Mo/Co/K zeolite and Mo/Ni/K zeolite: incipient wetness impregnation -Catalyst particle size: 0.45–0.8 mm (Fischer–Tropsch (FT) synthesis of aromatic hydrocarbons)	Stainless steel static reactor -Feed: (1) H_2/CO (50:50) (mol% H_2—46.76%, CO—47.41%, N_2—5.83%), (2) bio-syngas (mol%H_2—17.82%, N_2—46.03%, CO—22.65%, CH_4—1.76%, C_2H_4—0.25%, O_2—0.88%, CO_2—10.59%)	-The CO conversions of FT/Cu WGS catalytic systems were about 90% at 280 °C vs. 25% by using only FT catalyst.	[81]
Cu/CeO_2 Cu/ZrO_2 Cu/Al_2O_3 Cu/MgO	Co-precipitation -Cu loading = 20 wt% -Catalyst reduction: in 5% H_2/N_2 to 400 °C at a heating rate of 3.3 °C/min and	Fixed bed micro-tubular quartz reactor -Pressure: atmospheric -Temperature: 200–400 °C -GHSV: 36201 h^{-1} -Catalyst amount: 48 mg	-At 320 to 360 °C, CO conversion decreased as follow: $Cu/CeO_2 > Cu/MgO > Cu/ZrO_2 > Cu/Al_2O_3$ -At 200 °C, Cu/ZrO_2 exhibited the highest CO conversion.	[82]

Table 1 (continued)

Catalyst	Synthesized method	Experimental condition	Result	Ref
	remain in this temperature for 1 h before decreasing to 200 °C.	-Feed: 6.5 vol% CO, 7.1 vol% CO_2, 0.7 vol% CH_4, 42.4 vol% H_2, 28.7 vol% H_2O, and 14.5 vol% N_2.	-At 200 and 280 °C, co-precipitated Cu/CeO_2 catalyst had a higher conversion compared to the impregnated Cu/CeO_2 one (CO conversion at 200 °C: in the impregnated catalyst 8% and in the co-precipitated catalyst 30%).	
CeO_2/CuO (Ce:Cu atomic ratio = 4:6)	Reverse microemulsion -Catalyst peroxidation: at 573 K with 10 K min^{-1} rate for 30 min under 20% O_2/Ar	Tubular plug flow reactor -Temperature: 200–400 °C -Catalyst amount: 30 mg -Feed: 3% CO 3% H_2O, Ar balance -GHSV: 15000 h^{-1}	-Among the different identified species in this study, a type of carbonate species was found to be as a reaction intermediate.	[83]
Cu-CeO_2 Cu-HTlc	CeO_2 supports: precipitation HTlc support: commercial -catalyst pretreated: for 48 h at 275 °C under a nitrogen flow of 50 Ncm3/min	Packed tubular reactor -Pressure: atmospheric -Temperature: 125–295 °C -WHSV:1493–70,696 ml $h^{-1}g_{cat}^{-1}$	-At 125 and 175 °C, HTCu49 hybrid catalyst had the most activity (20–40% CO conversion) -At 175 °C and above, CeCu61 and CeCu43 catalysts presented the highest activity, reaching to 87.6 CO conversion and at 275 °C, 82.7% of CO conversions.	[84]
Cu-CeO_2 Cu-ZrO_2 Cu-CeO_2-ZrO_2	Co-precipitation -Cu loading: 20 wt%	Micro-tubular quartz reactor -Pressure: 1 atm -Temperature: 200–400 °C -GHSV: 72152 h^{-1} -Feed: 6.5 vol% CO, 7.1 vol% CO_2, 0.7 vol% CH_4, 42.4 vol% H_2, 28.7 vol% H_2O, and 14.5 vol% N_2	-The Cu-$Ce_{0.8}Zr_{0.2}O_2$ catalyst gave the highest conversion among all the prepared catalysts tested in this work. -Cu-$Ce_{0.8}Zr_{0.2}O_2$ catalyst had a stable activity at 320 °C for 100 h.	[85]
Cu-ZnO/Al_2O_3 Cu-ZnO/CeO_2-Al_2O_3	Wet impregnation -Catalyst preheated: at 500 °C for 4 h with a rate of 5 °C/min. -Catalyst reduction: under flowing H_2 at 50 mL/min rate for 1 h at 400 °C -Catalyst particle size: 200–300 μm	Fixed bed flow reactor -Pressure: atmospheric -Temperature: 150–350 °C -GHSV: 9000 h^{-1} -Feed: 30% vol. H_2O, 4.5% vol. CO, balance in He -Flow rate: 50 mL/min	-These developed Cu-based catalysts could operate successfully at relatively high SV close to reality suitable for portable applications. -Cu-ZnO/CeO_2-Al_2O_3 catalyst has the best behavior in terms of high stability as well as tolerance to start/stop conditions due to the presence of ceria preventing Cu from oxidation and sintering.	[86]
Cu/Ce/foam	-Foam was washed coated by ceria and copper phase was added by either wet impregnation or by urea-nitrates combustion -Cu loading: 4.5–7.0 wt%	Two coupled reactors -Temperature: 150–300 °C -GHSV: 3600–9500 h^{-1} -Feed: 47 vol% H_2, 27 vol% CO, 19 vol% CO_2, 2 vol% CH_4, and 5 vol% N_2 with an addition of water -Flow rate: 11.7 to 30.9 NL h^{-1} -S/C ratio: 2	- The wet impregnation method was found to be the optimized studied approach because it resulted in a similar activity to those more complex synthesis methods like urea-nitrate combustion.	[87]
Cu/ZnO/Al_2O_3	Co-precipitation -Catalyst pre-reduction: with pure H2 with 30 mL min − 1 rate at 573 K	Fixed bed reactor -Pressure: atmospheric -Temperature: 453 to 623 K	-The LDHs-30%Cu/Zn1Al as the optimum catalyst had much better performance in terms of initial	[88]

Table 1 (continued)

Catalyst	Synthesized method	Experimental condition	Result	Ref
	for 0.5 h and ten cooled down to 453 K	-GHSV: 8000 mL g^{-1} h^{-1} -Catalyst amount: 0.5 g -Feed: 15%CO/55% H_2/7%CO_2/N_2 -Flow rate: 66.7 mL min^{-1} -Vapor to dry feed gas ratio: 1	activity and stability, both thermal and long-term, than the commercial Cu/ZnO/Al_2O_3 catalyst.	
Cu-Fe_3O_4 Cu-Fe_3O_4-Al_2O_3	Aerosol spray self-assembly -Catalyst preheating: at 400 °C in air with the rate of 1 °C min^{-1} for 4 h. -Catalyst pretreated: with 5% H_2/Ar gas mixture for 30 min at 300 °C.	Fixed bed reactor -Pressure: 1 atm -Temperature: 150–400 °C -GHSV: 42000 mL g^{-1} h^{-1} -Catalyst amount: 100 mg -Feed: 2.2%CO/N_2 stream (56 cm^3 min^{-1}) mix with water vapor, and with CO and H_2O ration of 1:7	-The presence of Fe can highly disperse Cu and enhance WGS activity. -The tricomponent Cu-Fe_3O_4-Al_2O_3 catalyst is a promising prospect which can solve the problem of poor long-term stability existing with Cu-Fe_3O_4 at 250 °C.	[90]
Cu/Fe_3O_4	Aqueous precipitation -Both in the form of nanorods and nanoparticles -Catalyst reduction: by 5 vol% H_2/He gas at a flow rate of 30 mL/min at 300 °C for 2 h	Fixed bed continuous flow reactor -Pressure: atmospheric -GHSV: 40000 mL g^{-1} h^{-1} -Catalyst amount: 100 mg -Feed: 1% CO/3% H_2O/He	-Cu/Fe_3O_4 nanorods had no WGS reaction activity below 250 °C, while, Cu/Fe_3O_4 in nanoparticles form with the same Cu contents exhibited high low-temperature WGS activity.	[92]
Cu-Mn/SiO_2	Impregnation, co-precipitation and thermal decomposition of inorganic precursor complex -Catalyst reduction: at atmospheric pressure with a flow of H_2-N_2 ($N_2/H_2 = 1$; flow rate of each gas = 30 ml min^{-1}) at 400 °C for 6 h.	Fixed bed micro-reactor -Pressure: atmospheric -Temperature: 180–320 °C -GHSV: 3600 h^{-1} -Catalyst amount: 1000 mg -Feed: H_2O/CO (4:1)	-The decomposition preparation method is more appropriate making the catalyst highly dispersed resulting in higher activity and stability.	[93]
Co-based				
Co_3O_4 Alkali-promoted Co_3O_4	Incipient wetness impregnation	Fixed bed reactor -Pressure: atmospheric -Temperature: 453–573 K, -Catalyst amount: 0.2 g -Feed: 3.0% CO, 26.1% H_2O, 29.9% H_2, 3.7% N_2 (balance He)	-Co_2C was active for the WGS reaction however it deactivates with time on stream. -Na and K-promoted catalysts had much higher stability and activity than the other alkali-promoted Co_2C catalysts.	[100]
CoMo/Al_2O_3 (promoted CoMoS and unpromoted-MoS_2)	One-step pore-volume impregnation -Catalyst sulfidation: in 10% H_2S/H_2 up to 350 °C (3 °C/min) and keeping at 350 °C for 2 h.	Vertical fixed bed micro-reactor -Pressure: atmospheric -Temperature: 200–450 °C -GHSV: 2000 h^{-1} -Feed: 26 vol% CO, 54 vol% H_2 and 20 vol% CO_2 with water/gas molar ratio of 1	-At < 300 °C the intrinsic activity of un-MoS_2 site was by far smaller than promoted CoMoS one	[101]
Ni-based				
Ni-Ce-MFI	One-pot -Different percentages of Ni and Ce (0–3 wt%).	Fixed bed reactor -Pressure: atmospheric -Temperature: 453, 503, 533, 548, 563, and 593 K -GHSV: 0.099, 0.137, and 0.174 h^{-1}	-The Ce-MFI did not show any catalytic activity under the examined experimental conditions while the incorporated nickel samples could catalyze the reaction and the presence of Ce could provide the required O_2 to promote Ni and expedite the reaction.	[102]

Table 1 (continued)

Catalyst	Synthesized method	Experimental condition	Result	Ref
		-Feed (molar %): 10% CO, 15% H_2O, 4.8% Ar, and 70.2% He		
M/HAp (M: Ni, Cu, Co and Fe)	-The natural HAp-based support: calcination of pork chop bones -M/HAp catalysts: impregnation -Catalyst pretreating: at 450 °C for 2 h with a heating rate of 10 °C/min and air flow of 120 cm^3/min. -Catalyst reduction: in 60 cm^3/min flow of 15%H^2/He with a rate of 10 °C/min up to 400 °C keeping for 1 h then decreased to 150 °C in He flow.	Fixed bed reactor -Pressure: atmospheric -Catalyst amount: 0.1 g -Temperature: 100-450 °C -GHSV: 12000 h^{-1} -Feed: 1 vol% CO, 2 vol% H_2O, He balance -Flow rate: 200 cm^3/min -WSV = 2000 cm^3/g min (STP).	-Among all the investigated metals, Ni addition showed the highest catalytic performance in the WGS reaction (Ni > Co > Cu > Fe). -The activity and stability of the natural Ni/HAp was higher, and its methanation was lesser compared to synthetic HAp.	[103]
Ce support				
Pt/Ce	-Ceria support: sol–gel, combustion chemical vapor deposition, and, commercially obtained ceria. -Pt/Ce catalyst: reactive spray deposition technology (RSDT) equipment	BenchCAT™ 1000R HP -Temperature range: 150–450 °C -GHSV: 13360 h^{-1} -Feed: 0.94 vol% CO, 93 vol% Ar and 6 vol% water vapors	-The catalyst with the highest activity and well-dispersed Pt belonged to Pt/mesoporous ceria synthesized by sol-gel method with a complete conversion at 175 °C.	[105]
$Pt/Ce_{0.5}La_{0.5}O_{2-\delta}$	Sol-gel Pechini Urea co-precipitation -Catalyst preheated: at 600 °C with 20 vol% O_2/He for 2 h -Catalyst reduction: in H_2 (1 bar) at 300 °C for 2 h. -Catalyst particle size: 0.1–0.3 mm	-Temperature: 250–350 °C -Pressure: 1 atm -Feed: 3 vol% CO/10 vol% H_2O/87 vol% He -Flow rate: 200 N mL min^{-1}	-The catalyst prepared by urea co-precipitation method had higher activity compared to the other methods.	[107]
$Cu_xMn_{0.2-x}Ce_{0.8}O_2$ (x = 0–0.2) $Cu_{0.2}Ce_{0.8}O_2$	Nano-replication -Catalyst pretreating: in 10% H_2/He flow at 400 °C for 1 h, then cooling in He to 30 °C.	Fixed bed reactor -Temperature: 150–450 °C -Pressure: 1 atm -Catalyst amount: 0.06 g -Feed: 3% CO balanced with He and steam -Flow rate: 64 mL min^{-1}	-The $Cu_{0.2}Ce_{0.8}O_2$ catalyst had much higher WGS activity than the $Mn_{0.2-x}Ce_{0.8}O_2$ catalyst, and the co-incorporation of Cu and Mn enhanced the activity. -The $Cu_{0.18}Mn_{0.02}Ce_{0.8}O_2$ catalyst showed almost 100% of conversion with no methane production.	[113]
Au/ceria modified withY_2O_3 Au/CeO_2 (reference)	-Ceria supports modified by Y_2O_3: co-precipitation, wet impregnation -Au (3 wt%) catalysts: deposition-precipitation -Catalyst pretreating: at 200 or 350 °C in a flow of purified air for 1 h	Flow reactor -Temperature: 140–350 °C -Pressure: atmospheric -Feed: 3.37 vol% CO, 25.01 vol% H_2O and 71.62 vol% Ar -GHSV: 4000 h^{-1}	-Apart from $Au_{2.5}YCe$ prepared by the co-precipitation method, all other catalysts indicated more than 90% CO conversion at 180–220 °C. -Little superiority in the Au catalysts activity on YCe wet impregnation supports is due to the more contribution of the Au/Y_2O_3 nanostructures.	[108]
Cu/CeO_2	Normal/reverse precipitation and incipient wetness impregnation	Fixed bed micro-tubular quartz reactor -Temperature: 200–400 °C -Pressure: 1 atm	-The superior physicochemical properties of CeO_2 prepared by reverse precipitation greatly influenced the oxygen vacancy, dispersion of	[109]

Table 1 (continued)

Catalyst	Synthesized method	Experimental condition	Result	Ref
	-Catalyst pretreating: to 400 °C at the rate of 3.1 °C/min in a 5 vol% H_2/N_2, maintaining at this temperature for 1 h and after that decreasing to 200 °C.	-Catalyst amount: 48 mg -Feed: 9.0 vol% CO, 10.0 vol% CO_2, 1.0 vol% CH_4, 60.1 vol% H_2, and 19.9 vol% N_2 -GHSV: 36050 h^{-1}	Cu, and the catalyst reducibility of Cu/CeO_2 prepared by the reverse impregnation method. -The Cu/CeO_2 synthesized by reverse precipitation showed higher CO conversion than normal precipitation prepared one.	
CuO/CeO_2 (nanospheres (ns), nanorods (nr), and nanocubes (nc))	-ns: microemulsion -nr & nc: hydrothermal -Cu employing: incipient wetness impregnation	Micro-reactor -Temperature: 100–350 °C -Feed: 1% CO/ 3% steam/He -Flow rate: 10 ml min^{-1}	-The CuO/CeO_2 (ns) was the best catalyst among the other three studied samples in both activity and stability while CuO/CeO_2 (nc) exhibited poor activity and average stability.	[110]
CeO_2/CuO CeO_2/Mn-CuO	Precipitation -Mn: co-precipitation -Catalyst preheated: in 20% O_2/He mixture at 500 °C for 1 h	Fixed bed reactor -Pressure: atmospheric -Temperature: 200–500 °C -GHSV: 15000 h^{-1} -Catalyst amount: 1 g -Feed: 5% CO and 15% H_2O diluted in He -Flow rate: 250 cm^3 min^{-1} (STP)	-A Mn-induced improvement on the WGS activity was recognized. -The (Cu9Mn1)6Ce4 catalyst system showed more activity and Co conversion than Cu6Ce4 one, 70% vs. 60% at 200 °C.	[116]
Al support				
$Au/Al_2O_3/MnO_2/CuO$	-Al-supported Cu-Mn mixed oxides: wet impregnation -Au nanoparticles: deposition-precipitation	Flow reactor -Temperature: 120–260 °C -GHSV: 4000 h^{-1} -Feed: 3.37 vol% CO, 25.01 vol% H_2O, and 71.62 vol% Ar -Flow rate: 96 cm^3 min^{-1}	- The high catalytic activity of this system that practically useful is mostly because of economic viability by having 80% alumina in the system. -The useful role of Au nano-sized was not only the new active sites for CO activation, but it was also due to the CuO reducibility enhancement	[118]
Cu/Al_2O_3	-Mesoporous Al_2O_3 support: surfactant-assisted synthesis -Mesoporous Cu/ Al_2O_3 catalysts: conventional impregnation -Cu/metal oxide (Al_2O_3 and CeO_2) catalysts: co-precipitation -Catalyst reduction: flowing 20 vol% H_2/He gas with 30 cm^3 min^{-1} rate at 523 K for 2 h.	Fixed bed continuous flow reactor -Temperature: 473 K -GHSV: 5760 h^{-1} -Catalyst amount: 1 g -Feed: 9.5–10.2 vol% of CO, 22.4–43.9 vol% of H_2O, 39.8–60.1 vol% of H_2, and 6.8–7.3 vol% of CO_2 -Flow rate: 96 cm^3 min^{-1}	-In the S/C ratio of 2.2, the activity of Cu/Al_2O_3 catalyst enhanced with reducing mesopore size, whereas in the S/C ratio of 4.6, the catalytic activity promoted with increasing mesopore size.	[119]
Mo-Co/alkali/Al_2O_3	Commercial	Packed column -Temperature: 250–450 °C -GHSV: 10000 h^{-1} -Feed: CO of 45 vol%, CO_2 of 5 vol%, H_2 ~ 50 vol%,	-The Mo-Co/alkali/Al_2O_3 sulfur tolerant WGS catalyst could operate very steadily even with a steam/gas ratio of 0.2–0.3.	[122]

Table 1 (continued)

Catalyst	Synthesized method	Experimental condition	Result	Ref
		H_2S 3000 ppm, and N_2 (100 ml/min) a carrier gas -Flow rate: 50 ml/min -Steam/gas ratio: 0.7		
CuAlO/CuAl ceramometals (CuZnAl oxide for comparison)	Mechanochemical activation of a mixture of Cu: Al = 87: 13 wt% with subsequent Hydrothermal treatment	Catalyst bed reactor -Pressure: 1 bar -Temperature: 150–270 °C -Feed: CO:H2O:H_2 = 8:42:50 at a steam/gas ratio of 0.6–0.7	-The activity of granulated ceramometal was comparable with granulated CuZnAl oxide because of the high diffusion permeability	[124]
$Cu/ZnO/Al_2O_3$	-Conventional co-precipitation -Modified co-precipitation method (adding pseudo-boehmite to the suspension) -Catalyst reduction: at 220 °C for 60 min under a gas flow of 10% H_2 and 90% N_2.	Fixed bed reactor -Pressure: atmospheric -Catalyst amount: 0.2 g -Feed: 75 mol% H_2, 19 mol% CO_2 and 6 mol% CO -Flow rate: 2.7 L/h -vapor to CO molar ratio: 4.2:1.	The $Cu/ZnO/Al_2O_3$ catalyst synthesized by the modified method, showed much better activity and stability compared with the commercial sample.	[126]
Zr support				
$Pt/CeZrO_2$	$Ce_{0.25}Zr_{0.75}O_2$ and $Ce_{0.75}Zr_{0.25}O_2$: co-precipitation	Fixed bed quartz reactor -Temperature:150–400 °C for clean WGS reaction conditions, and 300 °C for sour condition 1 -Catalyst amount: 1 g -Feed: 5% H_2, 15% CO, 5% CO_2, 20% H_2O, and N_2 as balance. For sour condition, 50 ppm of H_2S was added -Flow rate: 100 mL/min -Catalyst amount: 250 mg	-In clean condition, catalysts such as CeO_2, $Ce_{0.75}Zr_{0.25}O_2$, and $Ce_{0.25}Zr_{0.75}O_2$ showed better primary catalytic activity because their supports were reducible, the capacity of oxygen storage and the concentration of basic sites. -The Pt/ $Ce_{0.25}Zr_{0.75}O_2$ showed the best option in sour condition among the studied catalysts due to higher catalytic activity, lower deactivation, and also full recovery potential.	[127]
CuZnAl PtCeAl AuCeAl	-CuZnAl catalyst: hydrotalcite like precursor after co-precipitation -PtCeAl: catalyst: wet impregnation -AuCeAl catalyst: direct anionic exchange (DAE)	Tubular fixed bed reactor -Temperature: 180–350 °C -Pressure: atmospheric -Feed: 4.5% CO, 30% of H_2O and N_2 -GHSV: 4000 h^{-1} -Catalyst amount: 0.16 g -Catalyst: ionic conductor mass ratio: 1:2	-The ZrEu ionic conductor was the most suitable one for the WGS reaction. -The activity of catalysts was CuZnAl > PtCeAl > AuCeAl	[129]
$Mo-S/ZrO_2$	Incipient wetness impregnation -Pre-sulfidation: 1 mol% H_2S in H_2 at 450 °C for 18 h.	Fixed bed tubular stainless steel micro-reactor -Pressure: atmospheric -Catalyst amount: 0.3–1.0 g -Feed: 10 vol% CO and 20 vol% H_2O in He -Flow rate: 35–85 mL/min -GHSV: 9000 mL/(g·h) -Temperature:150–300 °C	-The CO conversion of the catalyst improved with Mo content up to the monolayer coverage. -The $Mo-S/ZrO_2$ catalyst with the theoretical MoO3 monolayer coverage is highly promising for the WGS reaction run in the existence of sulfur-containing syngas impurities.	[131]
Si support				
$Pt-Mo/SiO_2$	Impregnation-reduction -0.1 g of reduced catalysts activated at 150 °C in H_2 for 2 h	Fixed bed Micro-reactor -Feed: 3% CO, 10% H_2O, balanced with He -Flow rate: 30 mL/min -GHSV: 18000 mL/(g·h) -Temperature:150–300 °C	-The Pt-Mo catalysts exhibited much higher activity than Pt/SiO_2 catalysts. -Adding Mo species enhances the Pt nanoparticles dispersion effectively.	[132]

Table 1 (continued)

Catalyst	Synthesized method	Experimental condition	Result	Ref
Cu/Si (aerogel and cubic mesostructured)	-Aerogels silica: supercritical drying of synthetic wet gels -Mesoporous silicas: surfactant-templated sol-gel synthetic Procedure -Catalyst: impregnating	Quartz-glass continuous flow fixed bed micro-reactor -Feed: 15 vol% CO, 40 vol% H_2O, balance N_2 -Flow rate: 25 cm^3 min^{-1} -WHSV: 4.60 h^{-1} -Temperature:150–400 °C	-The silica aerogel is a highly stable matrix in the catalytic cycles with a constant CO conversion	[133]
Ti support				
Au/TiO_2	-Double impregnation method (DIM) -Deposition-precipitation (DP) -Liquid phase reductive deposition (LPRD) -Catalyst pre-reduction: heating to 200 °C in N_2 and keeping it for 30 min. -Catalyst reduction: through feeding 15 vol% H_2/N_2 with a total flow rate of 50 ml_N/min for 45 min.	Packed-bed reactor -Feed: 4.76% CO, 10.06% CO_2, 28.46% H_2, 35.38% H_2O, 21.34% N_2 -Temperature: 150, 200, 250, and 300 °C. -SV:15 $L_N g_{cat}^{-1}$ h^{-1} -Pressure: atmospheric	-At temperature above 150 °C, both Au/TiO_2-LPRD and Au/TiO_2-DP with 2.36%Au, had better performance than the Au/TiO_2-WGC material. -In all the temperature, the Au/TiO_2-DP-2.36% showed the highest CO conversion reaching its maximum (~ 85%) at 300 °C. -Au nanoparticles of 1–5 nm have better activity.	[135]
Pd/TiO_2(K-PT)	Evaporation induced self-assembly -Catalyst reduction: in 5% H_2/He at 400 °C and maintaining for 1 h then decreased to room temperature.	Fixed bed reactor -Pressure: atmospheric -Catalyst amount: 0.06 g -Feed: 3.0%CO, 8.5% O_2 and He balance gas -Temperature: 200–450 °C -SV: 52000 $cm^3 g^{-1}_{cat}$ h^{-1} -Flow rate: 52 $cm^3 min^{-1}$	-Both PT and K-PT catalysts were highly active under the WGS reaction with 0% methane production. -Nanocrystalline particles and TiO2 support mesoporous enhanced the WGS activity.	[136]
Other metal support				
Pd/α-MnO_2 Pt/α-MnO_2	-α-MnO_2 support: hydrothermal method -Pd and Pt: precipitation -Catalysts: deposition-precipitation -Catalyst particle size: 40–60 mesh	Fixed bed flow Reactor -Pressure: atmospheric -Catalyst amount: 20 mg -Feed: 5 ml/min water steam along with 10% CO in Ar -Temperature: 140–350 °C -Flow rate:150 mL/min	-The catalysts activity comparable to Pd/CeO_2 and Pt/CeO_2.	[137]
Cu/MnO_x-CeO_2 Ni/MnO_x-CeO_2	-MnO_x-CeO_2 support: co-precipitation -Catalysts: impregnating support for 5 h at room temperature with Cu^{2+} or Ni^{2+}	Isothermal fixed bed glass reactor -Pressure: atmospheric -Feed: 8% of CO, 24% H_2O, 45% H_2, and N_2 as balance -Catalyst amount: 120 mg -Flow rate: 150 ml/min -Temperature: 250–450 °C	-CU catalysts supported on the low loading of Mn (CeMn30) showed higher reducibility and WGS activity compared to Cu catalysts prepared on the high Mn content support, while this trend was vice versa in case of nickel catalysts.	[138]
$PdO/MnO_x/CeO_2$-ZrO_2	Two-step impregnation -Catalyst reduction: in a flow of 10% H_2/Ar with a rate of 50 mL/min to 350 °C at 10 °C/min rate	Fixed bed quartz reactor -Pressure: atmospheric -Feed: 5 vol% CO, 10 vol% H_2O, and N_2 in balance -Catalyst amount: 100 mg	-At 325 °C the Mn-modified $PdO/Ce_{0.75}Zr_{0.25}O_2$ catalyst had 83% CO conversion in the WGS reaction with no CH_4 production, while this amount was only 36% over $PdO/Ce_{0.75}Zr_{0.25}O_2$	[140]

Table 1 (continued)

Catalyst	Synthesized method	Experimental condition	Result	Ref
	holding for 30 min in He (50 mL/min) to degas properly.	-GHSV: 12000 h^{-1} -Flow rate: 200 mL/min -Temperature: 250–350 °C	catalyst and no conversion obtained with the PdO/Al_2O_3 catalysts.	
CuMn/La	Coprecipitation -Catalyst particle size: 40–80 mesh	Tubular fixed bed stainless steel reactor -Pressure: atmospheric -Feed (volume fraction): 14.6% CO, 23.8% CO_2, 39.7% H_2, and Ar as balance -Catalyst amount: 0.5 g -SV: 6400 NmL/g·h -Steam/gas volume ratio: 0.6 -Temperature:150–300 °C	-The structure and properties of the studied catalysts were closely associated with the La content, and 0.5% La loading showed the best performance at low temperature for the WGS reaction.	[141]
CNT				
Pt/Na-C_N	Step-wise manner using carbon-modification -MWNT: commercial -Alkali metal addition: ion-exchange -Platinum deposition: incipient wetness impregnation	In-house packed-bed quartz micro-reactor -Pressure: atmospheric -Feed: 2% CO–10% H_2O–88% He -Catalyst amount: 0.1–0.2 g -Flow rate: 70 mL min^{-1}	-MWNTs oxidation by HNO_3 treatment before Pt addition results in a mild catalyst activation for WGS. -Na addition modifies the oxygen distribution on the catalyst surface significantly and considerably increases the activity.	[143]
Pt/Na-C_N	Co-impregnation -MWNT: commercial -Na promoter: impregnation -Pt-containing catalysts (1 wt% Pt): incipient wetness impregnation	Packed-bed quartz reactor -Pressure: atmospheric -Feed: (1) product-free 2% CO–10% H_2O–88% He (70 mL/min), (2) full reformate gas: 11% CO/25% H_2/25% H_2O/7% CO_2/32% He (150–210 mL/min) -Catalyst amount: 0.1–0.2 g	-Increasing in H_2 uptake was recognized on these materials by using both Pt and Na along with the catalyst.	[144]
Ni/CeO_2/CNT	-CNTs and activated carbon: commercial -Catalyst pretreatment: at 623 K form 5 h under flowing He with 50 mL min^{-1} flow rate. -Ce amount dispersion: 20 wt%	Fixed bed flow reactor -Pressure: atmospheric -Temperature: 413–533 K -Feed: (1) ideal: 1.87% CO, 35.92% H_2O, and He balance, (2) real: 7 mol% CO, 30 mol% H_2O, 50 mol% H_2, and 9 mol% CO_2 in He -Catalyst amount: 0.150 g -Flow rate: 100 mL min^{-1}	-The catalyst with fewer graphitic character exhibited better Ce dispersion and better Ni-Ce interaction, resulted in a greater catalytic performance. -The best catalysts with CNs based had better activity than those analogous catalyst synthesized over activated carbon	[145]
CNF				
Cu/CNF Cu/Al_2O_3	CNF support (macroscopic form): graphite felt immersing in HNO_3 -Catalyst: impregnating Cu in the support	Copper tubular reactor -Temperature:398–573 K	-The Cu/CNF catalyst had the highest activity in presence of the lowest evaluated value of p^{o}_{H2O} and H_2O:CO ratio of 3.	[147]
Graphene				
Ni/graphene Ni-CeO_2/graphene Ni/CeO_2 (for comparison)	-Graphite oxide (GO): from natural flake graphite by modified Hummers method -Catalysts: deposition-precipitation	Fixed bed flow reactor -Pressure: atmospheric -Temperature: 413–563 K -Feed: 1.87% CO, 35.92% H_2O, and He balance -Catalyst amount: 0.150 g	-The catalytic activity improved largely with sodium additive in ceria presence due to more oxygen vacancies, and better reducibility of the catalysts. -A very homogeneous nanoparticles dispersion was obtained by using Ni/G and Ni-CeO_2/G-Na.	[148]

Table 1 (continued)

Catalyst	Synthesized method	Experimental condition	Result	Ref
	-Catalyst reduction: during 1 h at 623 K with flowing H_2 at a rate of 50 mL min^{-1}	-Flow rate: 100 mL min^{-1}		
Other carbon-based catalyst				
$NiCeO_2/C$	$NiCeO_2/C$ catalyst: after conventional preparing, the catalyst was pretreated at 623 K for 4 h under flowing He (50 mL/min).	Fixed bed flow reactor -Pressure: atmospheric -Temperature: 413–633 K -Feed: (1) ideal: 1.75 mol% CO and 35.92 mol% H_2O in He, (2) actual: 1.75 mol% CO, 35.92 mol% H_2O, 34.45 mol% H_2, and 1.12 mol% CO_2 in He -Catalyst amount: 0.150 g -Flow rate: 100 mL/min	-The optimum amount of CeO_2 loading in ideal mixture was 20 wt% in which side reactions were not detected. -Under the real conditions, the catalyst with 10 wt% amount of CeO_2 showed the best performance.	[150]
Ni/CeO_2 (for comparison)	Ni/CeO_2 catalyst: homogeneous precipitation of CeO_2 and then impregnated with the Ni -Catalyst reduction: under flowing H_2 with a rate of 50 mL/min for 2 h at 623 K			

Table 2 Effect of different nanostructure and morphology of the catalysts towards WGSR

Nanostructure	Activity (T_{50})	Ref
Pt-SAC	285 °C	[36]
Pt nanoparticle	Does not reach 50% WGSR activity before 300 °C	
Au-cluster	200 °C	[60]
Au-particle	375 °C	
Cu-nanoparticles	High WGS activity	[92]
Cu-nanorods	No WGSR activity below 25^0C	
Ceria-nanosphere	320	[110]
Ceria-nanorod	337	
Ceria-nanocube	Does not reach 50% WGSR activity before 375 °C	

Application of ionic conductors in the support also provided encouraging results by enhancing the mobility of oxygen and vacant sites. The search for a low-cost catalyst with high activity, good hydrogen selectivity, and long-term stability will remain the focus from an economic point of view. Though many reports are available on the WGSR mechanism, the reaction pathway is still not very clear on many catalytic surfaces, particularly on catalysts with a low number of active sites. Efficient reactor design, along with catalyst development, will also play a critical role in this thermodynamically limited reaction. An optimal design will ensure quick removal of the products to push the reaction further by avoiding the reaching of thermodynamic equilibrium conditions.

Acknowledgements The author(s) would like to acknowledge support from Qatar University internal grant QUCG-CENG-19/20-7 for conducting this study. Authors would also like to acknowledge the open access funding provided by the Qatar National Library.

Funding Information Open Access funding provided by the Qatar National Library.

Compliance with ethical standards

Conflict of interest The authors declare that there are no conflicts of interest.

Abbreviations AC, activated carbon; ACP, aromatic conductive polymer; ASSA, aerosol spray self-assembly; CNF, carbon nano fibers; CNT, carbon nanotube; DFT, density functional theory; DI, double impregnation; EDX, energy dispersive X-ray; EG, ethylene glycol; GHSV, gas hourly space velocity; GO, graphene oxide; HAADF- STEM, high-angle annular dark-field scanning transmission electron microscopy; HAp, hydroxyapatite; HDP, homogeneous deposition precipitation; HRSTEM, high-resolution scanning transmission electron microscopy; HRTEM, high-resolution transmission electron microscopy; HTlc, hydrotalcite; IL, ionic liquid; I-R, impregnation-reduction; IWI, incipient wetness impregnation; LDHs, layered double hydroxides; LPRD, liquid phase reductive deposition; MFI, mordenite framework inverted; MWNTs, multi-walled carbon nanotubes; NC, nanocube; NR, nanorod; NS, nanospheres; OSC, oxygen storage capacity; PD, precipitation deposition; RM, reverse microemulsion; SAC, single-atom catalyst; SCFD, supercritical fluid

deposition; SEM, scanning electron microscopy; SFD, supercritical fluid deposition; SILP, supported ionic liquid phase; SV, space velocity; TEM, transmission electron microscopy; TOS, time on stream; TPD, temperature-programmed desorption; WGC, world gold council; WGS, water-gas shift; WGSR, water-gas shift reaction; WHSV, weight hourly space velocity; XRD, X-ray diffraction; ZIF-8, zeolitic imidazolate framework-8; ZSM-5, zeolite socony mobil–5

References

1. D. Pal et al., Performance of water gas shift reaction catalysts: a review. Renew. Sust. Energ. Rev. **93**, 549–565 (2018)
2. X. Chen, S. Shen, L. Guo, S.S. Mao, Semiconductor-based photocatalytic hydrogen generation. Chem. Rev. **110**(11), 6503–6570 (2010)
3. C. Rhodes, G. Hutchings, A. Ward, Water-gas shift reaction: finding the mechanistic boundary. Catal. Today **23**(1), 43–58 (1995)
4. M.D. Bhatt, J.S. Lee, Nanomaterials for photocatalytic hydrogen production: from theoretical perspectives. RSC Adv. **7**(55), 34875–34885 (2017)
5. S. Kahng, H. Yoo, J.H. Kim, Recent advances in earth-abundant photocatalyst materials for solar H2 production. Adv. Powder Technol. **31**(1), 11–28 (2020)
6. Y. Peng, P. Kan, Q. Zhang, Y. Zhou, Oxygen vacancy enhanced photoreduction Cr (VI) on few-layers BiOBr nanosheets. Catalysts **9**(6), 558 (2019)
7. H. Li, J. Shang, Z. Ai, L. Zhang, Efficient visible light nitrogen fixation with BiOBr nanosheets of oxygen vacancies on the exposed {001} facets. J. Am. Chem. Soc. **137**(19), 6393–6399 (2015)
8. Liu, S., et al., Promoting hydrogen evolution reaction through oxygen vacancies and phase transformation engineering on layered double hydroxide nanosheets. Journal of Materials Chemistry A, 2020
9. L. Gradisher, B. Dutcher, M. Fan, Catalytic hydrogen production from fossil fuels via the water gas shift reaction. Appl. Energy **139**, 335–349 (2015)
10. R.J. Byron Smith, M. Loganathan, M.S. Shantha, *A review of the water gas shift reaction kinetics*. Int. J. Chem. React. Eng., **8**(1) (2010)
11. Amos, W.A., *Biological water-gas shift conversion of carbon monoxide to hydrogen.* Milestone Completion Report, National Renewable Energy Laboratory (NREL) MP-560-35592, 2004
12. M. Dolan, S. Hla, L. Morpeth, Design and operational considerations for a catalytic membrane reactor incorporating a vanadium-based membrane. Sep. Purif. Technol. **147**, 398–405 (2015)
13. S.-E. Park, J.-S. Chang, K.-W. Lee, *Carbon Dioxide Utilization for Global Sustainability: Proceedings of the 7th International Conference on Carbon Dioxide Utilization* (Elsevier, *Seoul, Korea*, *October 12–16, 2003*, 2004)
14. C.Á. Galván et al., Reverse water-gas shift reaction at the Cu/ZnO interface: influence of the Cu/Zn ratio on structure-activity correlations. Appl. Catal. B Environ. **195**, 104–111 (2016)
15. H. Chu, Q. Li, A. Meng, Y. Zhang, Investigation of hydrogen production from model bio-syngas with high CO2 content by water-gas shift reaction. Int. J. Hydrog. Energy **40**(11), 4092–4100 (2015)
16. A. Alijani, A. Irankhah, Effect of nickel addition on ceria-supported platinum catalysts for medium-temperature shift reaction in fuel processors. Chem. Eng. Technol. **36**(4), 552–558 (2013)
17. K.-J. Kim, Y.L. Lee, H.S. Na, S.Y. Ahn, J.O. Shim, B.H. Jeon, H.S. Roh, Efficient waste to energy conversion based on co-ceo2 catalyzed water-gas shift reaction. Catalysts **10**(4), 420 (2020)
18. Brenna, G., *New catalysts for the H2 production by water-gas shift reaction processes*. 2011, alma
19. K. Sun, M. Kohyama, S. Tanaka, S. Takeda, Reaction mechanism of the low-temperature water–gas shift reaction on Au/TiO2 catalysts. J. Phys. Chem. C **121**(22), 12178–12187 (2017)
20. S.C. Ammal, A. Heyden, Water-gas shift activity of atomically dispersed cationic platinum versus metallic platinum clusters on titania supports. ACS Catal. **7**(1), 301–309 (2017)
21. A.A. Gokhale, J.A. Dumesic, M. Mavrikakis, On the mechanism of low-temperature water gas shift reaction on copper. J. Am. Chem. Soc. **130**(4), 1402–1414 (2008)
22. R. Bouarab, S. Bennici, C. Mirodatos, A. Auroux, Hydrogen production from the water-gas shift reaction on iron oxide catalysts. J. Catal. **2014**, 1–6 (2014)
23. N. Schumacher, A. Boisen, S. Dahl, A.A. Gokhale, S. Kandoi, L.C. Grabow, J.A. Dumesic, M. Mavrikakis, I. Chorkendorff, Trends in low-temperature water-gas shift reactivity on transition metals. J. Catal. **229**(2) 267–275 (2005)
24. S.C. Ammal, A. Heyden, Origin of the unique activity of Pt/TiO2 catalysts for the water–gas shift reaction. J. Catal. **306**, 78–90 (2013)
25. D. Trimm, Minimisation of carbon monoxide in a hydrogen stream for fuel cell application. Appl. Catal. A Gen. **296**(1), 1–11 (2005)
26. Z.I. Oensan, Catalytic processes for clean hydrogen production from hydrocarbons. Turk. J. Chem. **31**(5), 531–550 (2007)
27. C. Ratnasamy, J.P. Wagner, Water gas shift catalysis. Catal. Rev. **51**(3), 325–440 (2009)
28. Ç. Odabaşı, M.E. Günay, R. Yıldırım, Knowledge extraction for water gas shift reaction over noble metal catalysts from publications in the literature between 2002 and 2012. Int. J. Hydrog. Energy **39**(11), 5733–5746 (2014)
29. D. Andreeva, I. Ivanov, L. Ilieva, M.V. Abrashev, R. Zanella, J.W. Sobczak, W. Lisowski, M. Kantcheva, G. Avdeev, K. Petrov, Gold catalysts supported on ceria doped by rare earth metals for water gas shift reaction: influence of the preparation method. Appl. Catal. A Gen. **357**(2), 159–169 (2009)
30. P. Panagiotopoulou, D.I. Kondarides, Effect of the nature of the support on the catalytic performance of noble metal catalysts for the water–gas shift reaction. Catal. Today **112**(1–4), 49–52 (2006)
31. J. Vecchietti, A. Bonivardi, W. Xu, D. Stacchiola, J.J. Delgado, M. Calatayud, S.E. Collins, Understanding the role of oxygen vacancies in the water gas shift reaction on ceria-supported platinum catalysts. ACS Catal. **4**(6), 2088–2096 (2014)
32. R. Tiwari, B. Sarkar, R. Tiwari, C. Pendem, T. Sasaki, S. Saran, R. Bal, Pt nanoparticles with tuneable size supported on nanocrystalline ceria for the low temperature water-gas-shift (WGS) reaction. J. Mol. Catal. A Chem. **395**, 117–123 (2014)
33. H. Zhao, S. Yao, M. Zhang, F. Huang, Q. Fan, S. Zhang, H. Liu, D. Ma, C. Gao, Ultra-small platinum nanoparticles encapsulated

in Sub-50 nm hollow titania nanospheres for low-temperature water–gas shift reaction. ACS Appl. Mater. Interfaces **10**(43), 36954–36960 (2018)
34. A.I. Osman, J.K. Abu-Dahrieh, N. Cherkasov, J. Fernandez-Garcia, D. Walker, R.I. Walton, D.W. Rooney, E. Rebrov, A highly active and synergistic Pt/Mo2C/Al2O3 catalyst for water-gas shift reaction. Mol. Catal. **455**, 38–47 (2018)
35. Anil, C. and G. Madras, *Catalytic behaviour of Mn2. 94M0. 06O4-δ (M= Pt, Ru and Pd) catalysts for low temperature water gas shift (WGS) and CO oxidation*. International Journal of Hydrogen Energy, 2019
36. Y. Chen, J. Lin, L. Li, B. Qiao, J. Liu, Y. Su, X. Wang, Identifying size effects of Pt as single atoms and nanoparticles supported on FeO x for the water-gas shift reaction. ACS Catal. **8**(2), 859–868 (2018)
37. T.-D. Nguyen-Phan, A.E. Baber, J.A. Rodriguez, S.D. Senanayake, Au and Pt nanoparticle supported catalysts tailored for H2 production: from models to powder catalysts. Appl. Catal. A Gen. **518**, 18–47 (2016)
38. V. Palma et al., Catalytic activities of bimetallic catalysts for low temperature water gas shift reaction. Chem. Eng. Trans. **52**, 481–486 (2016)
39. J.W. Deal, P. le, C.B. Corey, K. More, C.W. West, Water-gas shift reaction on alumina-supported Pt-CeOx catalysts prepared by supercritical fluid deposition. J. Supercrit. Fluids **119**, 113–121 (2017)
40. A. Kaftan, M. Kusche, M. Laurin, P. Wasserscheid, J. Libuda, KOH-promoted Pt/Al2O3 catalysts for water gas shift and methanol steam reforming: an operando DRIFTS-MS study. Appl. Catal. B Environ. **201**, 169–181 (2017)
41. M. González-Castaño, S. Ivanova, O.H. Laguna, L.M. Martínez T., M.A. Centeno, J.A. Odriozola, Structuring Pt/CeO2/Al2O3 WGS catalyst: introduction of buffer layer. Appl. Catal. B Environ. **200**, 420–427 (2017)
42. A.S. Duke, K. Xie, A.J. Brandt, T.D. Maddumapatabandi, S.C. Ammal, A. Heyden, J.R. Monnier, D.A. Chen, Understanding active sites in the water–gas shift reaction for Pt–re catalysts on titania. ACS Catal. **7**(4), 2597–2606 (2017)
43. J.A. Rodriguez, P.J. Ramírez, R.A. Gutierrez, Highly active Pt/MoC and Pt/TiC catalysts for the low-temperature water-gas shift reaction: effects of the carbide metal/carbon ratio on the catalyst performance. Catal. Today **289**, 47–52 (2017)
44. M.A. Rivero-Crespo, M. Mon, J. Ferrando-Soria, C.W. Lopes, M. Boronat, A. Leyva-Pérez, A. Corma, J.C. Hernández-Garrido, M. López-Haro, J.J. Calvino, E.V. Ramos-Fernandez, D. Armentano, E. Pardo, Confined Pt11+ water clusters in a MOF catalyze the low-temperature water–gas shift reaction with both CO2 oxygen atoms coming from water. Angew. Chem. Int. Ed. **57**(52), 17094–17099 (2018)
45. R.V. Kumar, Y. Diamant, A. Gedanken, Sonochemical synthesis and characterization of nanometer-size transition metal oxides from metal acetates. Chem. Mater. **12**(8), 2301–2305 (2000)
46. J.L. Fajín, M.N.D. Cordeiro, Probing the efficiency of platinum nanotubes for the H2 production by water gas shift reaction: a DFT study. Appl. Catal. B Environ. **263**, 118301 (2020)
47. X. Sun, J. Lin, Y. Zhou, L. Li, Y. Su, X. Wang, T. Zhang, FeOx supported single-atom Pd bifunctional catalyst for water gas shift reaction. AICHE J. **63**(9), 4022–4031 (2017)
48. E. Kono, S. Tamura, K. Yamamuro, S. Ogo, Y. Sekine, Pd/K/Co-oxide catalyst for water gas shift. Appl. Catal. A Gen. **489**, 247–254 (2015)
49. M. Shekhar, J. Wang, W.S. Lee, M. Cem Akatay, E.A. Stach, W. Nicholas Delgass, F.H. Ribeiro, Counting Au catalytic sites for the water–gas shift reaction. J. Catal. **293**, 94–102 (2012)
50. C.M. Yeung, S.C. Tsang, A study of co-precipitated bimetallic gold catalysts for water–gas shift reaction. Catal. Commun. **9**(7), 1551–1557 (2008)
51. M.G. Castaño et al., *Pt vs. Au in water–gas shift reaction*. J. Catal. **314**, 1–9 (2014)
52. M. González-Castaño, T. R. Reina, S. Ivanova, L.M. Martínez Tejada, M.A. Centeno, J.A. Odriozola, O2-assisted water gas shift reaction over structured Au and Pt catalysts. Appl. Catal. B Environ. **185**, 337–343 (2016)
53. M. Soria et al., Effect of the preparation method on the catalytic activity and stability of Au/Fe2O3 catalysts in the low-temperature water–gas shift reaction. Appl. Catal. A Gen. **470**, 45–55 (2014)
54. S. Yao, X. Zhang, W. Zhou, R. Gao, W. Xu, Y. Ye, L. Lin, X. Wen, P. Liu, B. Chen, E. Crumlin, J. Guo, Z. Zuo, W. Li, J. Xie, L. Lu, C.J. Kiely, L. Gu, C. Shi, J.A. Rodriguez, D. Ma, Atomic-layered Au clusters on α-MoC as catalysts for the low-temperature water-gas shift reaction. Science **357**(6349), 389–393 (2017)
55. T. Reina et al., The role of Au, Cu & CeO_2 and their interactions for an enhanced WGS performance. Appl. Catal. B Environ. **187**, 98–107 (2016)
56. B.S. Çağlayan, A.E. Aksoylu, Water–gas shift activity of ceria supported Au–Re catalysts. Catal. Commun. **12**(13), 1206–1211 (2011)
57. G.N. Özyönüm, R. Yildirim, Water gas shift activity of Au–Re catalyst over microstructured cordierite monolith wash-coated by ceria. Int. J. Hydrog. Energy **41**(12), 5513–5521 (2016)
58. Q. Fu, H. Saltsburg, M. Flytzani-Stephanopoulos, Active nonmetallic Au and Pt species on ceria-based water-gas shift catalysts. Science **301**(5635), 935–938 (2003)
59. J. Santos et al., Gold promoted Cu/ZnO/Al2O3 catalysts prepared from hydrotalcite precursors: advanced materials for the WGS reaction. Appl. Catal. B Environ. **201**, 310–317 (2017)
60. X.-P. Fu, L.W. Guo, W.W. Wang, C. Ma, C.J. Jia, K. Wu, R. Si, L.D. Sun, C.H. Yan, Direct identification of active surface species for the water–gas shift reaction on a gold–ceria catalyst. J. Am. Chem. Soc. **141**(11), 4613–4623 (2019)
61. C.E. Stere, J.A. Anderson, S. Chansai, J.J. Delgado, A. Goguet, W.G. Graham, C. Hardacre, S.F.R. Taylor, X. Tu, Z. Wang, H. Yang, Non-thermal plasma activation of gold-based catalysts for low-temperature water–gas shift catalysis. Angew. Chem. Int. Ed. **56**(20), 5579–5583 (2017)
62. J. Santos et al., Multicomponent au/cu-ZnO-Al2O3 catalysts: robust materials for clean hydrogen production. Appl. Catal. A Gen. **558**, 91–98 (2018)
63. A. Goguet, R. Burch, Y. Chen, C. Hardacre, P. Hu, R.W. Joyner, F.C. Meunier, B.S. Mun, D. Thompsett, D. Tibiletti, Deactivation mechanism of a Au/CeZrO4 catalyst during a low-temperature water gas shift reaction. J. Phys. Chem. C **111**(45), 16927–16933 (2007)
64. D. Tibiletti, A. Amieiro-Fonseca, R. Burch, Y. Chen, J.M. Fisher, A. Goguet, C. Hardacre, P. Hu, D. Thompsett, DFT and in situ EXAFS investigation of gold/ceria− zirconia low-temperature water gas shift catalysts: identification of the nature of the active form of gold. J. Phys. Chem. B **109**(47), 22553–22559 (2005)
65. J.H. Carter, P.M. Shah, E. Nowicka, S.J. Freakley, D.J. Morgan, S. Golunski, G.J. Hutchings, Enhanced activity and stability of gold/ceria-titania for the low-temperature water-gas shift reaction. Frontiers in chemistry **7** (2019)
66. H. Guan, J. Lin, B. Qiao, S. Miao, A.Q. Wang, X. Wang, T. Zhang, Enhanced performance of Rh1/TiO2 catalyst without methanation in water-gas shift reaction. AICHE J. **63**(6), 2081–2088 (2017)
67. X.-F. Yang, A. Wang, B. Qiao, J. Li, J. Liu, T. Zhang, Single-atom catalysts: a new frontier in heterogeneous catalysis. Acc. Chem. Res. **46**(8), 1740–1748 (2013)

68. R. Mandapaka, G. Madras, Aluminium and rhodium co-doped ceria for water gas shift reaction and CO oxidation. Molecular Catalysis **451**, 4–12 (2018)
69. B. Liu, T. Huang, Z. Zhang, Z. Wang, Y. Zhang, J. Li, The effect of the alkali additive on the highly active Ru/C catalyst for water gas shift reaction. Catal. Sci. Technol. **4**(5), 1286–1292 (2014)
70. P.C. Ford, The water gas shift reaction: homogeneous catalysis by ruthenium and other metal carbonyls. Acc. Chem. Res. **14**(2), 31–37 (1981)
71. T. Huang, B. Liu, Z. Zhang, Y. Zhang, J. Li, Preparation of confined Ru-iongel catalysts and their application for a low temperature water–gas shift reaction. RSC Adv. **4**(54), 28529–28536 (2014)
72. Queiroz, G., C. Barbosa, and C. Abreu, *Production of hydrogen by water-gas shift reaction on Ru/C catalyst.* Brazilian Journal of Petroleum and Gas, 2018. **12**(2)
73. Queiroz, G., C. Barbosa, and C. Abreu, *Low-temperature water-gas shift reaction with Ru/TiO2 and Ru/Al2O3 catalysts.* Brazilian Journal of Petroleum and Gas, 2016. **10**(3)
74. G.A. de Queiroz, C.M.B. de Menezes Barbosa, C. A. Pimentel, C.A.M. de Abreu, Performance of the water gas shift process with a ruthenium catalyst for hydrogen production in a membrane reactor. React. Kinet. Mech. Catal. **123**(2), 679–687 (2018)
75. S. Werner, N. Szesni, A. Bittermann, M.J. Schneider, P. Härter, M. Haumann, P. Wasserscheid, Screening of supported ionic liquid phase (SILP) catalysts for the very low temperature water–gas-shift reaction. Appl. Catal. A Gen. **377**(1–2), 70–75 (2010)
76. S. Werner, N. Szesni, R.W. Fischer, M. Haumann, P. Wasserscheid, Homogeneous ruthenium-based water–gas shift catalysts via supported ionic liquid phase (SILP) technology at low temperature and ambient pressure. Phys. Chem. Chem. Phys. **11**(46), 10817–10819 (2009)
77. R. Stepić, C.R. Wick, V. Strobel, D. Berger, N. Vučemilović-Alagić, M. Haumann, P. Wasserscheid, A.S. Smith, D.M. Smith, Mechanism of the water–gas shift reaction catalyzed by efficient ruthenium-based catalysts: a computational and experimental study. Angew. Chem. Int. Ed. **58**(3), 741–745 (2019)
78. M.Á. Centeno Gallego et al., Boosting the activity of a Au/CeO2/Al2O3 catalyst for the WGS reaction. Catal. Today **253**, 149–154 (2015)
79. P. Liu, J.A. Rodriguez, Water-gas-shift reaction on metal nanoparticles and surfaces. J. Chem. Phys. **126**(16), 164705 (2007)
80. M.A. Saqlain, A. Hussain, D.M. Siddiq, O. Leenaerts, A.A. Leitão, DFT study of synergistic catalysis of the water-gas-shift reaction on Cu–Au bimetallic surfaces. ChemCatChem **8**(6), 1208–1217 (2016)
81. R. Wijayapala, F. Yu, C.U. Pittman Jr., T.E. Mlsna, K-promoted Mo/Co-and Mo/Ni-catalyzed Fischer–Tropsch synthesis of aromatic hydrocarbons with and without a Cu water gas shift catalyst. Appl. Catal. A Gen. **480**, 93–99 (2014)
82. D.-W. Jeong, W.J. Jang, J.O. Shim, W.B. Han, H.S. Roh, U.H. Jung, W.L. Yoon, Low-temperature water–gas shift reaction over supported Cu catalysts. Renew. Energy **65**, 102–107 (2014)
83. A.L. Cámara, S. Chansai, C. Hardacre, A. Martínez-Arias, The water–gas shift reaction over CeO2/CuO: operando SSITKA–DRIFTS–mass spectrometry study of low temperature mechanism. Int. J. Hydrog. Energy **39**(8), 4095–4101 (2014)
84. M.N. Moreira, A.M. Ribeiro, A.F. Cunha, A.E. Rodrigues, M. Zabilskiy, P. Djinović, A. Pintar, Copper based materials for water-gas shift equilibrium displacement. Appl. Catal. B Environ. **189**, 199–209 (2016)
85. D.-W. Jeong, H.S. Na, J.O. Shim, W.J. Jang, H.S. Roh, A crucial role for the CeO 2–ZrO 2 support for the low temperature water gas shift reaction over Cu–CeO 2–ZrO 2 catalysts. Catal Sci. Technol. **5**(7), 3706–3713 (2015)
86. C. Price, L. Pastor-Pérez, E. le Saché, A. Sepúlveda-Escribano, T.R. Reina, Highly active Cu-ZnO catalysts for the WGS reaction at medium–high space velocities: effect of the support composition. Int. J. Hydrog. Energy **42**(16), 10747–10751 (2017)
87. C. Lang, X. Sécordel, C. Courson, Copper-based water gas shift catalysts for hydrogen rich syngas production from biomass steam gasification. Energy Fuel **31**(11), 12932–12941 (2017)
88. D. Li, S. Xu, Y. Cai, C. Chen, Y. Zhan, L. Jiang, Characterization and catalytic performance of Cu/ZnO/Al2O3 water–gas shift catalysts derived from Cu–Zn–Al layered double hydroxides. Ind. Eng. Chem. Res. **56**(12), 3175–3183 (2017)
89. Z. Zhang, S.S. Wang, R. Song, T. Cao, L. Luo, X. Chen, Y. Gao, J. Lu, W.X. Li, W. Huang, The most active Cu facet for low-temperature water gas shift reaction. Nat. Commun. **8**(1), 488 (2017)
90. Han Yan, X.-T.Q., Yue Yin, Yun-Fei Teng, Zhao Jin, Chun-Jiang Jia, *Promoted Cu-Fe3O4 catalysts for low-temperature water gas shift reaction: optimization of Cu content.* Applied Catalysis B: Environmental, 2018: p. 182–193
92. L. Zhao, Y. Qi, L. Song, S. Ning, S. Ouyang, H. Xu, J. Ye, Solar-driven water–gas shift reaction over CuOx/Al2O3 with 1.1% of light-to-energy storage. Angew. Chem. Int. Ed. **58**(23), 7708–7712 (2019)
93. L. Ma, H. Ma, D. Han, M. Qiu, Y. Guan, Y. Hu, Evolution of copper supported on Fe3O4 nanorods for WGS reaction. Catalysts **8**(10), 415 (2018)
94. J. Farzanfar, R. Rezvani, Inorganic complex precursor: preparation of Cu-Mn/SiO2 mixed oxide nanocatalyst for low-temperature water-gas shift reaction. J. Sci. Islamic Repub Iran **29**(4), 321–333 (2018)
95. H. Yin, J. Shang, J. Choi, A.C.K. Yip, Generation and extraction of hydrogen from low-temperature water-gas-shift reaction by a ZIF-8-based membrane reactor. Microporous Mesoporous Mater. **280**, 347–356 (2019)
96. P. Kowalik, K. Antoniak-Jurak, R. Bicki, W. Próchniak, P. Wiercioch, K. Michalska, The alcohol-modified CuZnAl hydroxycarbonate synthesis as a convenient preparation route of high activity Cu/ZnO/Al2O3 catalysts for WGS. Int. J. Hydrog. Energy **44**(2), 913–922 (2019)
97. E. Jang, E. Kim, H. Kim, T. Lee, H.J. Yeom, Y.W. Kim, J. Choi, Formation of ZIF-8 membranes inside porous supports for improving both their H2/CO2 separation performance and thermal/mechanical stability. J. Membr. Sci. **540**, 430–439 (2017)
98. H. Yin, H. Kim, J. Choi, A.C.K. Yip, Thermal stability of ZIF-8 under oxidative and inert environments: a practical perspective on using ZIF-8 as a catalyst support. Chem. Eng. J. **278**, 293–300 (2015)
99. Chen, L., J. Zhang, and X. Liang, *Reducing gas atmosphere (H2, CO) assisted formation of Fe-Ce-Ox composite oxides with enhanced catalytic activity for water-gas shift reaction.* Catal. Commun., 2019: p. 105849
100. T.R. Reina, S. Ivanova, V. Idakiev, J.J. Delgado, I. Ivanov, T. Tabakova, M.A. Centeno, J.A. Odriozola, Impact of Ce–Fe synergism on the catalytic behaviour of Au/CeO2–FeO x/Al2O3 for pure H2 production. Catal. Sci. Technol. **3**(3), 779–787 (2013)
101. M.K. Gnanamani, G. Jacobs, W.D. Shafer, D.E. Sparks, S. Hopps, G.A. Thomas, B.H. Davis, Low temperature water–gas shift reaction over alkali metal promoted cobalt carbide catalysts. Top. Catal. **57**(6–9), 612–618 (2014)
102. J. Chen, J. Zhang, J. Mi, E.D. Garcia, Y. Cao, L. Jiang, L. Oliviero, F. Maugé, Hydrogen production by water-gas shift reaction over Co-promoted MoS2/Al2O3 catalyst: the intrinsic activities of Co-promoted and unprompted sites. Int. J. Hydrog. Energy **43**(15), 7405–7410 (2018)

103. S. Alamolhoda, G. Vitale, A. Hassan, N.N. Nassar, P.P. Almao, Synergetic effects of cerium and nickel in Ce-Ni-MFI catalysts on low-temperature water-gas shift reaction. Fuel **237**, 361–372 (2019)
104. U. Iriarte-Velasco, J.L. Ayastuy, Z. Boukha, R. Bravo, M.Á. Gutierrez-Ortiz, Transition metals supported on bone-derived hydroxyapatite as potential catalysts for the water-gas shift reaction. Renew. Energy **115**, 641–648 (2018)
105. A. Luengnaruemitchai, S. Osuwan, E. Gulari, Comparative studies of low-temperature water–gas shift reaction over Pt/CeO2, Au/CeO2, and Au/Fe2O3 catalysts. Catal. Commun. **4**(5), 215–221 (2003)
106. R. Jain, A.S. Poyraz, D.P. Gamliel, J. Valla, S.L. Suib, R. Maric, Comparative study for low temperature water-gas shift reaction on Pt/ceria catalysts: role of different ceria supports. Appl. Catal. A Gen. **507**, 1–13 (2015)
107. C.K. Byun, H.B. Im, J. Park, J. Baek, J. Jeong, W.R. Yoon, K.B. Yi, Enhanced catalytic activity of Cu/Zn catalyst by Ce addition for low temperature water gas shift reaction. Clean Technology **21**(3), 200–206 (2015)
108. K.C. Petallidou, S. Boghosian, A.M. Efstathiou, *Low-temperature water–gas shift on Pt/Ce0. 5La0. 5O2− δ: effect of support synthesis method*. Catal. Today **242**, 153–167 (2015)
109. T. Tabakova, L. Ilieva, I. Ivanov, M. Manzoli, R. Zanella, P. Petrova, Z. Kaszkur, Structure-activity relationship in water-gas shift reaction over gold catalysts supported on Y-doped ceria. J. Rare Earths **37**(4), 383–392 (2019)
110. H.-S. Na, J.O. Shim, S.Y. Ahn, W.J. Jang, K.W. Jeon, H.M. Kim, Y.L. Lee, K.J. Kim, H.S. Roh, Effect of precipitation sequence on physicochemical properties of CeO2 support for hydrogen production from low-temperature water-gas shift reaction. Int. J. Hydrog. Energy **43**(37), 17718–17725 (2018)
111. S. Yao et al., Morphological effects of the nanostructured ceria support on the activity and stability of CuO/CeO2 catalysts for the water-gas shift reaction. Phys. Chem. Chem. Phys. **16**(32), 17183–17195 (2014)
112. C. Schilling, C. Hess, Elucidating the role of support oxygen in the water–gas shift reaction over ceria-supported gold catalysts using operando spectroscopy. ACS Catal. **9**(2), 1159–1171 (2018)
113. D. Gu et al., Ordered mesoporous cu–Ce–O catalysts for CO preferential oxidation in H2-rich gases: influence of copper content and pretreatment conditions. Appl. Catal. B Environ. **152**, 11–18 (2014)
114. C. Li, Z. Li, H.Y. Oh, G.H. Hong, J.S. Park, J.M. Kim, Ordered mesoporous Cu-Mn-Ce ternary metal oxide catalysts for low temperature water-gas shift reaction. Catal. Today **307**, 237–242 (2018)
115. X. Huang, M.J. Beck, Determining the oxidation state of small, hydroxylated metal-oxide nanoparticles with infrared absorption spectroscopy. Chem. Mater. **27**(8), 2965–2972 (2015)
116. X. Huang, M.J. Beck, Metal-free low-temperature water–gas shift catalysis over small, hydroxylated ceria nanoparticles. ACS Catal. **5**(11), 6362–6369 (2015)
117. A.L. Cámara et al., Novel manganese-promoted inverse CeO2/CuO catalyst: in situ characterization and activity for the water-gas shift reaction. Catal. Today **339**, 24–31 (2020)
118. Cámara, A.L., V.C. Corberán, and A. Martínez-Arias, Inverse CeO2/CuO WGS catalysts: influence of the presence of oxygen in the reactant mixture. Catal. Today, 2019
119. T. Tabakova, I. Ivanov, Y. Karakirova, D. Karashanova, A. Venezia, P. Petrova, G. Avdeev, E. Kolentsova, K. Ivanov, Promotional effect of gold on the WGS activity of alumina-supported copper-manganese mixed oxides. Catalysts **8**(11), 563 (2018)
120. K. Sagata, Y. Kaneda, H. Yamaura, S. Kobayashi, H. Yahiro, Influence of coexisting Al2O3 on the activity of copper catalyst for water–gas-shift reaction. Int. J. Hydrog. Energy **39**(35), 20639–20645 (2014)
121. D.S. Newsome, The water-gas shift reaction. Catal. Rev. Sci. Eng. **21**(2), 275–318 (1980)
122. D. Nikolova et al., The state of (K)(Ni) Mo/γ-Al2O3 catalysts after water–gas shift reaction in the presence of sulfur in the feed: XPS and EPR study. Appl. Catal. A Gen. **297**(2), 135–144 (2006)
123. B. Liu et al., Recent advances in industrial sulfur tolerant water gas shift catalysts for syngas hydrogen enrichment: application of lean (low) steam/gas ratio. Catalysts **9**(9), 772 (2019)
124. S.F. Tikhov, V.A. Sadykov, K.R. Valeev, A.N. Salanov, S.V. Cherepanova, Y.N. Bespalko, V.E. Ramanenkau, Y.Y. Piatsiushyk, S.V. Dimov, Preparation of porous ceramometal composites through the stages of mechanical activation and hydrothermal partial oxidation of Me–Al powders. Catal. Today **246**, 232–238 (2015)
125. S. Tikhov, T. Minyukova, K. Valeev, S. Cherepanova, A. Salanov, V. Kaichev, A. Saraev, A. Andreev, O. Lapina, V. Sadykov, Design of micro-shell Cu–Al porous ceramometals as catalysts for the water–gas shift reaction. RSC Adv. **7**(67), 42443–42454 (2017)
126. S. Tikhov et al., Particularities of low-temperature WGSR over ceramometal and oxide catalysts: effect of catalyst particle size. Chem. Eng. J. **374**, 405–411 (2019)
127. L. Xu, D. Peng, W. Liu, Y. Feng, Y. Hou, X. Li, C. Huang, A modified co-precipitation method to prepare Cu/ZnO/Al 2 O 3 catalyst and its application in low temperature water-gas shift (LT-WGS) reaction. J Wuhan Univ Technol.-Mater. Sci. Ed. **33**(4), 876–883 (2018)
128. L.P. Silva et al., Sour water–gas shift reaction over Pt/CeZrO2 catalysts. J. Catal. **341**, 1–12 (2016)
129. Wang, X., et al., *In situ time-resolved characterization of Au–Ce O 2 and Au O x–Ce O 2 catalysts during the water-gas shift reaction: presence of Au and O vacancies in the active phase*. 2005, American Institute of Physics
130. N. García-Moncada, M. González-Castaño, S. Ivanova, M.Á. Centeno, F. Romero-Sarria, J.A. Odriozola, New concept for old reaction: novel WGS catalyst design. Appl. Catal. B Environ. **238**, 1–5 (2018)
131. M. González-Castaño, S. Ivanova, T. Ioannides, M.A. Centeno, J.A. Odriozola, Deep insight into Zr/Fe combination for successful Pt/CeO 2/Al 2 O 3 WGS catalyst doping. Catal. Sci. Technol. **7**(7), 1556–1564 (2017)
132. Yun, S. and V. Guliants, *Surface coverage effects on water gas shift activity of ZrO2 supported Mo sulfide catalysts.* Catal. Commun., 2019: p. 105810
133. X. Xu, Q. Fu, X. Bao, MoOx-promoted Pt catalysts for the water gas shift reaction at low temperatures. Chin. J. Catal. **36**(5), 750–756 (2015)
134. C. Marras, D. Loche, D. Carta, M.F. Casula, M. Schirru, M.G. Cutrufello, A. Corrias, Copper-based catalysts supported on highly porous silica for the water gas shift reaction. ChemPlusChem **81**(4), 421–432 (2016)
135. S. Carrettin, M.C. Blanco, A. Corma, A.S.K. Hashmi, Heterogeneous gold-catalysed synthesis of phenols. Adv. Synth. Catal. **348**(10–11), 1283–1288 (2006)
136. P. Pérez et al., *Application of Au/TiO2 catalysts in the low-temperature water–gas shift reaction*. Int. J. Hydrog. Energy **41**(8), 4670–4681 (2016)
137. C. Li, K. Sivaranjani, J.M. Kim, Synthesis of alkali promoted mesoporous, nanocrystalline Pd/TiO2 catalyst for water gas shift reaction. Catal. Today **265**, 45–51 (2016)
138. J.-J. Shan et al., *Water–gas shift on Pd/α-MnO 2 and Pt/α-MnO 2*. Catal. Lett. **145**(8), 1571–1580 (2015)
139. E. Poggio-Fraccari, J. Sambeth, G. Baronetti, F. Mariño, Cu/MnOx–CeO2 and Ni/MnOx–CeO2 catalysts for the water–gas

shift reaction: metal–support interaction. Int. J. Hydrog. Energy **39**(16), 8675–8681 (2014)
140. X. Wang, R.J. Gorte, J. Wagner, Deactivation mechanisms for Pd/ceria during the water–gas-shift reaction. J. Catal. **212**(2), 225–230 (2002)
141. Y. Xiao, X. Wu, S. Liu, J. Wan, M. Li, D. Weng, C. Tong, Modification of PdO/CeO 2–ZrO 2 catalyst by MnO x for water–gas shift reaction: redox property and valence state of Pd. J. Mater. Sci. **51**(11), 5377–5387 (2016)
142. H. Runxia et al., Cu-Mn catalysts modified by rare earth lantnaum for low temperature water-gas shift reaction. J. Rare Earths **34**(10), 994–1003 (2016)
143. Serp, P. and B. Machado, *Nanostructured carbon materials for catalysis*. 2015: Royal Society of Chemistry
144. B. Zugic, D.C. Bell, M. Flytzani-Stephanopoulos, Activation of carbon-supported platinum catalysts by sodium for the low-temperature water-gas shift reaction. Appl. Catal. B Environ. **144**, 243–251 (2014)
145. B. Zugic, S. Zhang, D.C. Bell, F.(.F.). Tao, M. Flytzani-Stephanopoulos, Probing the low-temperature water–gas shift activity of alkali-promoted platinum catalysts stabilized on carbon supports. J. Am. Chem. Soc. **136**(8), 3238–3245 (2014)
146. A.B. Dongil et al., Carbon nanotube-supported Ni–CeO2 catalysts. Effect of the support on the catalytic performance in the low-temperature WGS reaction. Carbon **101**, 296–304 (2016)
147. F. Huber, Z. Yu, J.C. Walmsley, D. Chen, H.J. Venvik, A. Holmen, Nanocrystalline Cu-Ce-Zr mixed oxide catalysts for water-gas shift: carbon nanofibers as dispersing agent for the mixed oxide particles. Appl. Catal. B Environ. **71**(1–2), 7–15 (2007)
148. N. Oliveira, G.P. Valençaa, R. Vieirab, Water gas shift reaction on copper catalysts supported on alumina and carbon nanofibers. Chem. Eng. **43**, 931–936 (2015)
149. A.B. Dongil, L. Pastor-Pérez, A. Sepúlveda-Escribano, P. Reyes, Promoter effect of sodium in graphene-supported Ni and Ni–CeO2 catalyst for the low-temperature WGS reaction. Appl. Catal. A Gen. **505**, 98–104 (2015)
150. A. Dongil et al., Chemoselective hydrogenation of cinnamaldehyde: a comparison of the immobilization of Ru–phosphine complex on graphite oxide and on graphitic surfaces. J. Catal. **282**(2), 299–309 (2011)
151. L. Pastor-Pérez, R. Buitrago-Sierra, A. Sepúlveda-Escribano, *CeO2-promoted Ni/activated carbon catalysts for the water–gas shift (WGS) reaction*. Int. J. Hydrog. Energy **39**(31), 17589–17599 (2014)
152. L. Pastor-Pérez, T. Reina, S. Ivanova, M. Centeno, J. Odriozola, A. Sepúlveda-Escribano, Ni-CeO2/C catalysts with enhanced OSC for the WGS reaction. Catalysts **5**(1), 298–309 (2015)
153. S. Collins, G. Finos, R. Alcántara, E. del Rio, S. Bernal, A. Bonivardi, Effect of gallia doping on the acid–base and redox properties of ceria. Appl. Catal. A Gen. **388**(1–2), 202–210 (2010)
154. T. Chapman, The hydrogen economy blasts off. Physics world **15**(7), 29 (2002)
155. Pistikopoulos, E.N., M.C. Georgiadis, and A. Kokossis, *21st European Symposium on Computer Aided Process Engineering*. 2011: Elsevier